8-30-2011

Synthesis and nano-mechanical characterization of calcium silicate hydrate (C-S-H)

Emilia Foley

Recommended Citation

Foley, Emilia. "Synthesis and nano-mechanical characterization of calcium silicate hydrate (C-S-H)." (2011).
https://digitalrepository.unm.edu/ce_etds/43

Emilia M Foley
Candidate

Civil Engineering
Department

This thesis is approved, and it is acceptable in quality and form for publication:

Approved by the Thesis Committee:

Mahmoud Reda Taha , Chairperson

Arup Maji

Maria Juenger

Synthesis and Nano-Mechanical Characterization of Calcium Silicate Hydrate

by

Emilia Michelle Foley

B.S., Civil Engineering, University of New Mexico, 2009

THESIS

Submitted in Partial Fulfillment of the
Requirements for the Degree of

Master of Science
Civil Engineering

The University of New Mexico

Albuquerque, New Mexico

July 2011

Dedication

To my parents: I wouldn't be where I am today if not for your continual and unyielding emotional and financial support over the course of my 7 years of education. I could never ask for a better, more supportive family.

Acknowledgments

A big thank you first and foremost to the Defense Threat Reduction Agency for funding my graduate education and research. None of this research would have been achieved without their financial support.

Dr. Mahmoud Reda Taha: Thank you for the opportunity to work for you, your guidance, and your support throughout graduate school. I feel very fortunate to have worked under you for the last 3 years.

Kenny Martinez: Thank you for all the times you helped me solve logistics and set-up issues for my experiments in the lab. I would have had a lot more blunders and failed experiments if it weren't for you!

Dr. Timothy Ross: You initially told me about the opportunity to work with Dr. Taha back when I was still an undergraduate. If it weren't for you, I wouldn't have ever started working for Dr. Taha and consequently probably wouldn't have ever gone to graduate school at all.

Michael Sheyka: Thank you for all your hard work performing my nanoindentation tests. My thesis wouldn't have been possible without your help!

Dr. Jung Kim: Thank you for all your help with statistical deconvolution analysis and formatting of my figures and papers. It was of enormous help.

Preface

During the course of this thesis (2008-2011) the following papers have been submitted for publication in scholarly journals:

1) Foley, E., Kim, J.J., Reda Taha, M.M. "Synthesis and Nano-Mechanical Characterization of C-S-H with a 1.5 C/S Ratio", *Cement and Concrete Research*, in review, 2011.

2) Foley, E., Kim, J.J., Reda Taha, M.M. "Synthesis and Nano-Mechanical Characterization of C-S-H at multiple C/S Ratios", *Materials and Structures*, in preparation, 2011.

The following abstract was presented in conference proceedings:

"Synthesis and Nano-mechanical Characterization of C-S-H", Emmy Foley, presented at American Concrete Institute conference, October 2010.

Synthesis and Nano-Mechanical Characterization of Calcium Silicate Hydrate

by

Emilia Michelle Foley

ABSTRACT OF THESIS

Submitted in Partial Fulfillment of the
Requirements for the Degree of

Master of Science
Civil Engineering

The University of New Mexico

Albuquerque, New Mexico

July 2011

Synthesis and Nano-Mechanical Characterization of Calcium Silicate Hydrate

by

Emilia Michelle Foley

B.S., Civil Engineering, University of New Mexico, 2009
M.S., Civil Engineering, University of New Mexico, 2011

Abstract

Calcium Silicate Hydrate (C-S-H) constitutes two-thirds of hydrated cement paste by volume. Having a better understanding of the mechanical properties of C-S-H will significantly aid in future effort for making 'concrete by design' for specific applications such as blast resistance. C-S-H is an amorphous compound whose chemical structure has been debated by researchers for years. It has been found that C-S-H can form with a wide variety of calcium to silicate (C/S) ratios, and it is the intent of this thesis to determine the effect of the C/S ratio on mechanical properties, most specifically elastic modulus of C-S-H. By varying the calcium and silicate ratios as well as the density of the material, relationships can be formulated between these properties and the mechanical properties of the material. As C-S-H is an amorphous substance, its chemical composition can vary widely depending on the ratio of the raw materials mixed and the water-cement ratio. Here, C-S-H is synthesized at room temperature and atmospheric pressure by producing calcium oxide (CaO) using calcium carbonate and then mixing it with fumed silica (SiO_2) and enough deionized water to make slurry. The slurry was continuously mixed for 7 days, after which the excess water was removed. C/S ratios of 1.5, 1.2, and 0.9 were synthesized. In addition, C-S-H with a C/S ratio of 1.5 was synthesized under high temperature (80°C) and pressure (10 MPa, 98.7 atm). The resultant C-S-H was dried to a set water level using two standard techniques known as D-drying and equilibration to 11% relative humidity (RH). The C-S-H was then chemically and mechanically characterized. The dried powders were characterized using thermogravimetric analysis (TGA), x-ray diffraction analysis (XRDA), and ^{29}Si magic angle spinning nuclear magnetic resonance (MAS-NMR) spectroscopy. The characterization confirmed the formation of C-S-H with high purity. It also identified the level of silicate polymerization and its correlation to the stiffness of C-S-H. The powders were then compacted to create specimens with porosities similar to C-S-H in cement. The specimens underwent nanoindentation experiments to mechanically characterize C-S-H. These experiments provide insight on the nanoscale mechanical characteristics of C-S-H. We then try to establish some links between the C-S-H composition and its mechanical properties.

Contents

List of Figures

List of Tables

Chapter 1

Introduction

Calcium Silicate Hydrate (C-S-H) comprises roughly two-thirds of hydrated cement paste by volume [1]. Throughout this thesis, C denotes lime, CaO, S denotes SiO_2, and H stands for water, H_2O. While there has been much research into mechanical properties of hydrated, heterogeneous cement and concrete, little work has been done to characterize the individual phases. Of the work done, much is still on hydrated cement samples, with methods being employed to single out the C-S-H phase in testing. One issue with these tests is the morphology and composition of the C-S-H. Unlike calcium hydroxide, which makes up about 25% of cement [1], C-S-H is amorphous and does not have a set chemical formula. Several sources report that the formula is $C_{1.7}SH_4$ [2, 1], while others contend a formula of $C_{1.5}SH_{1.5}$ [3, 4]. In reality, these are more just average values of the overall C-S-H, as it has been shown that C-S-H can form with a wide array of C/S ratios given the proper lime, silica, and water contents [5, 6, 7, 8]. In addition to this wide variation in chemical composition, it is generally accepted that C-S-H forms with two general densities, dubbed low-density and high-density [9, 10, 11]. The low-density phase is believed to make up two-thirds of the C-S-H [9], while the high-density phase comprises the remaining third. These definitions of density are rather loose; there are not two specific hard-and-fast densities to which C-S-H conforms. Again, like the stoichiometry, these density classifications are more of an average for the overall C-S-H matrix. To make things worse, the water bound inside C-S-H can also take a variety of forms. Water can be free, absorbed, or chemically bound. This makes C-S-H classification even more challenging. In order to alter a cement's overall mechanical response to loading, including elastic response, energy adsorption, and hardness, the mechanical properties of C-S-H need to be well-understood. Altering both the chemical composition and the density should undoubtedly alter the mechanical properties of the C-S-H and consequently the cement. Another important motivation is that characterizing C-S-H individually will enable recognizing C-S-H behavior when observed under nanoindentation. This is currently critical and unavailable information needed to analyze hydrated cement indentation results. The synthesis and characterization of C-S-H will enable more educated analysis of hydrated cement indentation data. Finally, the synthesis and characterization of C-S-H will produce knowledge necessary for next-generation binders such as geomaterials. Understanding how the silicate polymerization affects energy absorption and strength development in cement binders is a key to developing new classes of cement binders in the future.

Until now, the only data on the nano-scale properties of C-S-H have been collected on indentations of hydrated cement pastes. Utilizing statistical deconvolution techniques, C-S-H strength values were extrapolated using information known on the volume fraction of C-S-H. However, phase-pure C-S-H has never been mechanically tested to confirm or deny these findings. This work presents new research on the characterization of the mechanical properties of phase-pure C-S-H and its linkage to microstructural properties of C-S-H.

The objective of this work is to lay the groundwork for future synthesis of "concrete by design"–making concrete for specific purposes, such as blast resistance. Here, C-S-H was synthesized at several C/S ratios known to be achievable under normal curing conditions, and also synthesized under elevated temperature and pressure conditions to examine the effect of increased polymerization on the mechanical response of the material. The synthetic C-S-H material was made as a loose powder, which was then compacted into discs with a wide array of densities to try and mimic the C-S-H as it would be present in-situ in cement. After a gamut of chemical testing to confirm the formation and purity of the C-S-H, including Thermogravimetric Analysis, ^{29}Si Magic-Angle Spinning Nuclear Magnetic Resonance, and X-ray Diffraction Analysis, nanoindentation was employed to determine the effect of density and stoichiometry on the mechanical response of the material.

This work begins with a literature review covering past work on synthesis of C-S-H, drying and humidity conditioning performed on cement and C-S-H, surface preparation techniques used for nanoindentation, nanoindentation testing and other small-scale characterization of cement and C-S-H, and chemical characterization of cement and C-S-H. Next, the experimental methods used for synthesis, sample preparation, chemical characterization, and mechanical characterization are discussed. Following, the results of the chemical characterization proving the formation of C-S-H are presented along with the results of the nanoindentation tests, along with comments on the results. Finally, conclusions are drawn on the work and planned future work is discussed.

Chapter 2

Literature Review

2.1 Synthesis of C-S-H

Beaudoin and Feldman [12] synthesized C-S-H by producing aqueous solutions of sodium metasilicate and calcium oxide (quicklime) at various ratios. Six samples were made with C/S ratios between 0.68 and 1.49 and H/S ratios between 1.91 and 6.69. The samples were dried by bathing in acetone and ether followed by being placed under a steady stream of nitrogen for 4 days followed finally by being placed in a nitrogen environment for 1 day. The researchers determined water content using loss on ignition at 1000° C. The H/S ratios for the high C/S ratio C-S-H mixtures were found to be much higher than the researchers expected and higher than previously published values by Taylor [13]. Taylor suggested 2 types of C-S-H: C-S-H(I), with C/S ratios between 0.8 and 1.33, and C-S-H(II) with C/S ratios between 1.5 and 2.

Atkins et al. [8] synthesized C-S-H by mixing calcium oxide with either silicic acid or silica fume and distilled water. C/S ratios ranging between 0.9 and 1.7 were used. The samples were repeatedly filtered and re-dispersed to remove any impurities and dried to 30% relative humidity using saturated calcium chloride. No mechanical characterization was performed on this C-S-H. Rather, the researchers tested the solubility of the C-S-H along with other cement phases.

Cong and Kirkpatrick[7] synthesized C-S-H using 3 different methods: first by progressive hydration of β -C_2S, second by reacting CaO with fumed silica at C/S ratios between 0.4 and 2.0 with excess water for 2 months, and third by reacting fumed silica with β-C_2S with C/S ratios between 0.6 and 1.7 with 5 mL of water rotated for 10 months. Through XRD and ^{29}Si NMR investigations, the researchers observed a limiting C/S ratio for single-phase C-S-H as being around 1.5. Above this ratio, CH was detectable in XRD analysis, indicating an excess of CaO for the available SiO_2 to react with.

Sugiyama and Fujita [5] recently synthesized C-S-H at C/S ratios of 0.65, 0.83, 0.9, 1.1, and 1.2. The synthesis was performed by mixing calcium oxide with amorphous silica and distilled water. The mixes were hydrated for 7 days and dried under vacuum above silica gel. X-ray diffraction of their samples indicated pure C-S-H.

Alizadeh and Beaudoin [6] also recently synthesized C-S-H by mixing amorphous silica with calcium oxide in excess water. The calcium oxide was obtained by calcining calcium carbonate at 900°C. Samples with C/S ratios of 0.8, 1.0, 1.2, and 1.5 were mixed continuously for 6 months, even though it is noted that the reaction is nearly complete after 1 week. After hydration, the C-S-H was filtered and dried under vacuum for 4 days then conditioned for 3 weeks to an 11% relative humidity condition.

2.2 Drying and Humidity Conditioning of Cement and C-S-H

In 1971, Feldman and Ramachandran [14] hydrated Type I Portland cement for 1.5 years in a bottle at a w/c ratio of 5. The sample was then dried to 11% relative humidity. Part of the sample was further dried to the D-dry condition described in 1953 by Copeland and Hayes [15]. Comparing the water contents of the two conditioned samples, Feldman found that the 11% RH cement sample had roughly 3% more water than the D-dry conditioned sample. In addition to the D-dry and 11% RH cement samples, a third sample was prepared by drying under vacuum at 70°C for 2 hours. The 3 samples were then split up with portions being equilibrated at 11%, 32%, 44%, 58%, 66%, 76%, 84%, and 100% RH. After this stage, the samples were re-equilibrated to 11%RH. From these experiments, it was concluded that the water loss experienced by a cement sample down to the 11%RH condition is completely reversible. When a sample dried down to 11%RH is put into an environment of higher humidity, it reabsorbs the amount of moisture proportional to that humidity condition. Samples dried to the D-dry condition also reabsorb water, but must be exposed to humidity above 75% before the rehydration is complete. The 11%RH condition is therefore thought to be significant because at or around this state, only a monolayer of water is present in the C-S-H with no remaining capillary water.

Alizadeh and Beaudoin [6] conditioned C-S-H samples for 3 weeks to 11% relative humidity in a desiccator using a saturated lithium chloride solution. The reason for the selection of this water state is that it only leaves a monolayer of adsorbed water on the surface of the particles in addition to the interlayer water. This surface water aids in the compaction of the C-S-H powder and represent a key part of C-S-H microstructure.

2.3 Structure, Composition, and Water Content of C-S-H

Early investigation of the chemical composition of C-S-H was done by Kantro et al. [16]. C_2S and C_3S were hydrated at a W/C ratio of 0.7 for times ranging from 1 to 400 days at hydration temperatures of 5°C, 25°C, and 50°C. The samples were then ground and D-dried following the procedure given by Copeland and Hayes [15].

Kantro's tests found the C/S ratio of C-S-H in the C_2S paste to be 1.58 for the room-temperature (25°C) specimen. The C/S ratio was found to be 1.48 for the C-S-H in the hydrated C_3S paste for the room-temperature (25°C) specimen.

Later, Odler and Dorr [17] hydrated C_3S at W/C ratios of 0.7 and 0.5 for times ranging between 15 minutes and 48 hours. D-drying was employed to stop hydration at the desired times. CH content was calculated by thermogravimetric analysis. The C-S-H content and formulation was determined by subtracting the amount of CH from the amount of hydration product. The resulting formulas for C-S-H formed by C_3S hydration were found to be $C_{1.6}SH_{1.32}$ and $C_{1.99}SH_{1.71}$ for each CH content determination method, respectively. For direct comparison to Kantro, these formulas give C/S ratios of 1.6 and 1.99. These formulae are for C-S-H with only non-evaporable water, that is, water remaining after D-drying.

More recent research has investigated the variation in the forms and in-situ density of C-S-H within cement. Constantinides and Ulm [9] postulated that the C-S-H matrix in cement is made up of bulk low-density C-S-H with inclusions of high-density C-S-H dispersed throughout. It is also concluded that the volume fractions of high-density and low-density C-S-H depend primarily on the w/c ratio, with a ratio of 70% low-density to 30% high-density for a w/c of .5. A colloid model by Jennings [11] proposed a formula of $C_{1.7}SH_{0.7}$ for 11% humidity conditioned C-S-H.

2.4 Chemical Analysis of Cement and C-S-H

2.4.1 Thermogravimetric Analysis

Thermogravimetric analysis (TGA) tests are quite useful for determining calcium hydroxide (CH) and calcium carbonate contents as well as determining the purity of C-S-H. Several researchers have investigated cement paste using TGA with varying results. Alonso and Fernandez [18] made cement paste specimens with ordinary Portland cement at a w/c ratio of 0.4, cured for 70 days. Their TGA work concluded loss of water from C-S-H occurs from 100-250°C, loss of bound water from CH begins at 450°C, and finally decomposition of calcium carbonate begins around 650°C. Curves published in this paper depicting a reference Portland cement as well as cement dried to certain temperatures prior to TG analysis are shown in Figure 2.1. Alarcon-Ruiz et al. [19] found the range for water loss from C-S-H to be 100°-200°C. CH water loss is reported from 450-500°C, and calcium carbonate decomposition beginning at 750°C. Odelson et al. [20] prepared Type III cement paste samples and reported the range of mass loss from C-S-H to be between 200°C and 350°C. Jain and Neithalath [21] prepared cement paste samples at a w/c ratio of 0.4, hydrated for 8 weeks. C-S-H water loss was taken as the range from 150°C- ∼400°C (or the temperature at which water loss from CH begins). Mass loss was observed from 400-450°C for the mass loss from CH. This analysis technique is further discussed in section 3.5 and provide some insight on TG analysis of C-S-H.

Earnest [22] published the curve seen in Figure 2.2, which is a typical TGA curve for Ordinary Portland Cement. The initial mass loss between 300K and 700K (∼25°C to ∼425°) represents water loss from C-S-H. The large, steep drop from 700K to ∼730K (∼425°C to ∼460°) is representative of the decomposition of CH. Unlike the curves published by Alonso, this sample appears to have no carbonation, which appears as a mass loss due to CO_2 disassociating from $CaCO_3$ in the range of 600°C to 800°C (875K-1000K).

A complication not discussed with these TG analyses is water loss from AFt and AFm phases such as ettringite and the hydration products of the aluminates and sulfates. These losses would occur at a low temperature, in the same range as C-S-H water loss. This makes extracting the percent of C-S-H more difficult and the mass loss range more complicated to determine.

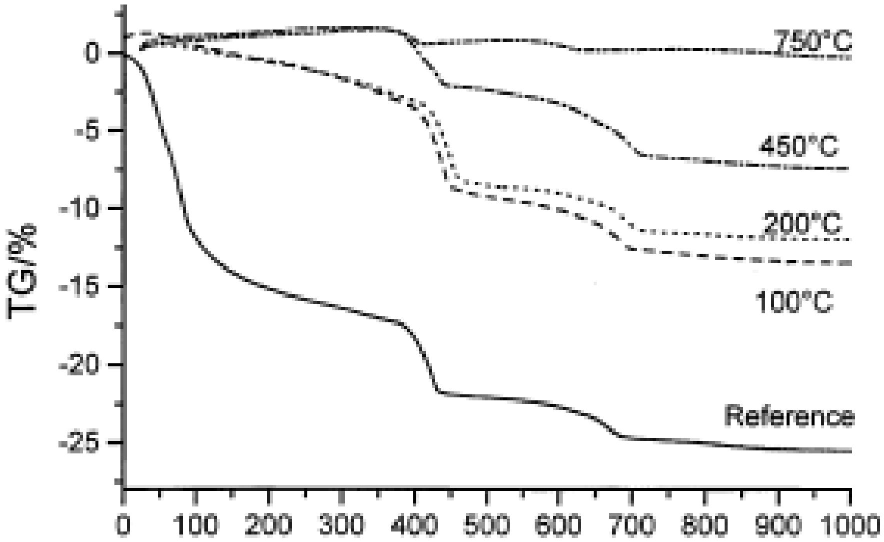

Figure 2.1: Typical TGA curve for Ordinary Portland Cement as published by Alonso and Fernandez [18].

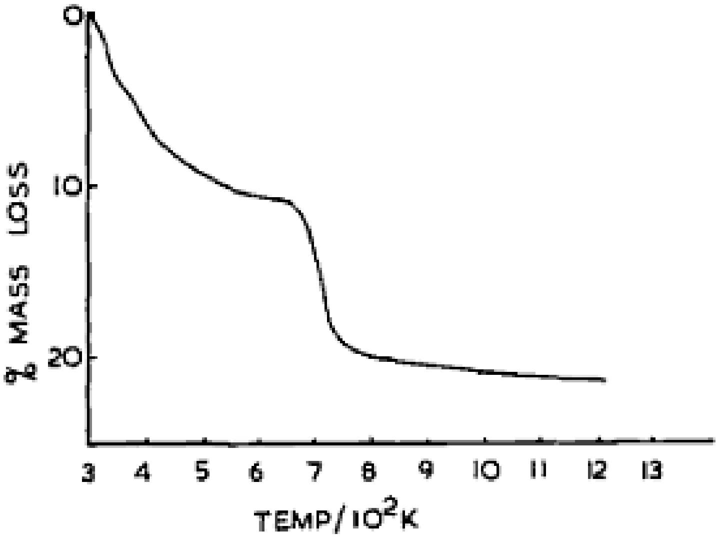

Figure 2.2: Typical TGA curve for Ordinary Portland Cement as published by Earnest [22].

2.4.2 ^{29}Si Magic-Angle Spinning Nuclear Magnetic Resonance (MAS-NMR)

^{29}Si MAS-NMR is a useful tool for analyzing the chemical connectivity and polymerization of silica-based compounds. Peaks made by the sample are compared to peaks formed by a standard reference sample (usually pure Si for the ^{29}Si test). The difference between peaks is defined as the chemical shift and is typically multiplied by 10^6 and given units of parts per million (ppm). Q^n notation is used to express the number of bridging molecules (oxygen in this case) connecting multiple Si molecules together. Q^0 denotes no bridging, which is observed in unhydrated cement. Q^1, Q^2, Q^3, and Q^4 denote increasing polymerization, where pure Q^4 is observed for pure silica fume and sand. Figure 2.3 shows the ^{29}Si chemical shift ranges as published by Magi et al. [23].

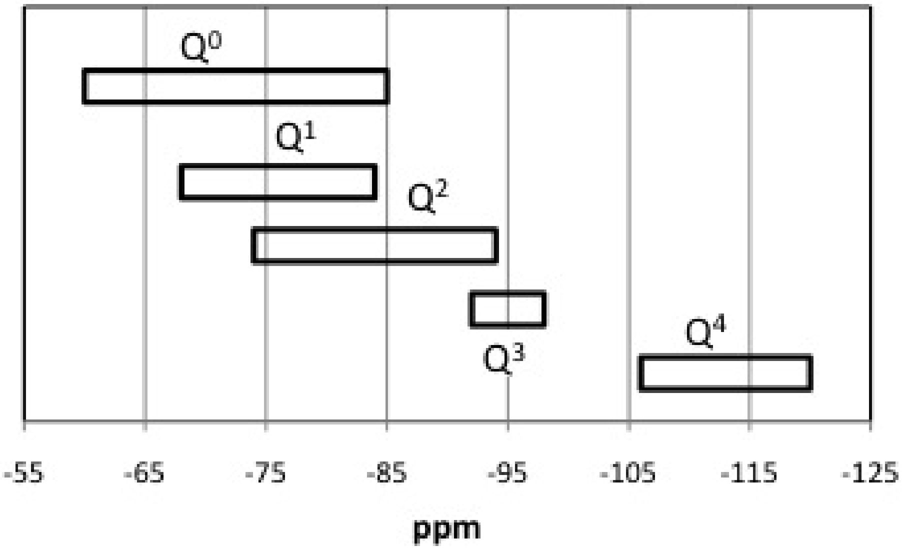

Figure 2.3: ^{29}Si chemical shift ranges of silicates as published by Magi et al. [23].

Young [24] reported an increase in polymerization, and consequently a chemical shift in ^{29}Si NMR peaks, when cement pastes were cured under elevated temperatures compared to samples cured under room temperature. Young [24] hydrated C_3S and white Portland cement samples at 2°C, 25°C, and 65°C and, after curing, dried the samples to 105°C before testing with NMR. Samples were spun at 2 kHz. For samples cured at 2°C and 25°C, over half of the sample was observed to have Q^1 bond, while samples cured at 65°C showed a shift to an increased abundance of Q^2 bond, which indicates longer silicate chains. Q^1 sites show a peak at -79.5 ppm and Q^2 sites show a peak at -85.3 ppm. Amorphous silica would appear as a Q^3 site, peaking at -99 ppm and -102 ppm. The degree of polymerization in the C-S-H samples is said to be expressed by the ratio $Q^1/\sum Q^i$. A higher number indicates less polymerization.

Cong and Kirkpatrick [7] synthesized C-S-H using 3 methods: first by progressive hydration of β-C_2S, second by reacting CaO with fumed silica at C/S ratios between 0.4 and 2.0 with excess water for 2 months, and third by reacting fumed silica with β-C_2S with C/S ratios between 0.6 and 1.7 with 5 mL of water rotated for 10 months. Samples from each method were packed in 7mm rotors and spun at 4 kHz. Samples with the lowest C/S ratio (0.97 for the first preparation method, 0.41 for the second method, and 0.6 for the final method) show most if not all Q^2 bonding. The highest C/S ratios (1.85, 1.7, and 1.85, for each method, respectively) show a much stronger tendency toward Q^1 silicate chains. All intermediate C/S values shift proportionally between these two extremes, with C/S ratios of 1.77 and 1.27 having near-equal ratios of Q^1 and Q^2 chains for the first preparation method. Samples prepared using fumed silica and β-C_2S showed that samples with C/S ratios between 1.2 and 1.5 have near-equal ratios of Q^1 and Q^2 chains. Experimental results [7] showed average degrees of polymerization of 0.32, 0.48, and 0.7 for C/S ratios of 1.0, 1.2, and 1.5, respectively.

Results presented by Alonso and Fernandez [18] showed peaks for Q^0, Q^1, and Q^2 for a hydrated cement paste. Q^0 peaks are due to unhydrated cement. All ^{29}Si NMR peaks should be representative of only C-S-H, as SiO_2 is only expected to be present in C-S-H. Findings show 55% Q^1, 35% Q^2, and 10% Q^0. Q^0 is attributed only to anhydrous cement. Beaudoin et al. [25] prepared pure synthetic C-S-H samples with C/S ratios of 0.6, 0.8, 1.0, 1.2, 1.5, and 1.6. Samples were hydrated for up to 1 year followed by drying for 4 days under vacuum. Samples were packed in 7 mm rotors and spun at 4.5 kHz. For C-S-H with a 1.6 C/S ratio, almost all the sample is made up of Q^1 bonding, indicating weak polymerization. The sample with C/S of 1.0 shows near-equal Q^1 and Q^2 bonding, and the 0.6 C/S sample shows nearly all Q^2 bonding, with a small but unmistakably present peak of Q^3 bonding, indicating cross-linking between the chain layers.

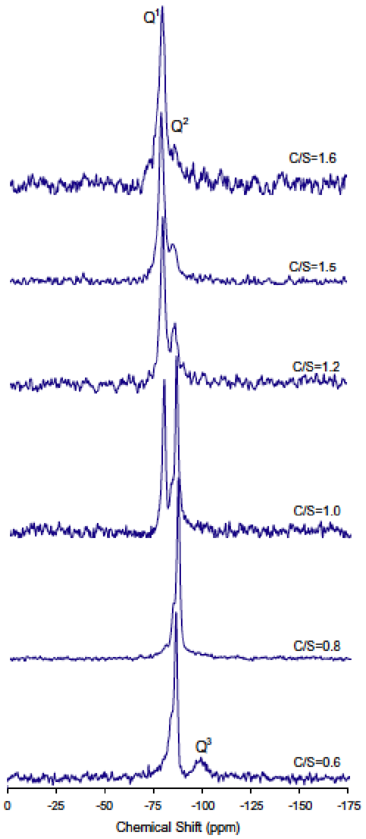

Figure 2.4: ^{29}Si NMR results published by Beaudoin et al. [25]

Beaudoin et al. [25] synthesized C-S-H with C/S ratios of 0.6, 0.8, 1.0, 1.2, 1.5, and 1.6 and used ^{29}Si NMR for characterization of the silica bonds, as shown in

Figure 2.4. This figure clearly shows a shift of the Q^1 and Q^2 peaks. For high C/S ratios, almost all silicate bonding is Q^1. For the very low C/S ratio of 0.6, there is no observed Q^1, and actually a small amount of Q^3 observed, showing significantly more polymerization than the higher C/S ratio materials. For all intermediate steps, there is a clear shift towards more Q^2 bonding as C/S ratio decreases.

Le Saout et al. [26, 27] found that the average degree of SiO_4 tetrahedra connectivity, $\bar{n}$, can be found using Equation 2.1. The Q^n values input into this equation are the relative volume fractions as percentages.

$$\bar{n} = \frac{Q^1 + 2Q^2 + 3Q^3}{Q^1 + Q^2 + Q^3} \tag{2.1}$$

The mean chain length, L, is the number of silicates bound together in a chain. This is typically found using the Q^2/Q^1 ratio shown equation 2.2.

$$L = 2 * (1 + \frac{Q^2}{Q^1}) \tag{2.2}$$

Taylor [28] examined the chain lengths of naturally occurring calcium silicate hydrates jennite and tobermorite. Jennite has a basic formula of $C_9S_6H_{11}$ (C/S=1.5) and tobermorite has a basic formula of $C_5S_6H_5$ (C/S=0.83) [28]. For these particular formulae, the chain lengths are theoretically infinite. When the chains are missing some of the silica tetrahedra bridging the groups together, finite chain lengths result. This also alters the chemical composition. The reported variation in chain length and chemical composition of jennite and tobermorite are shown in Figure 2.5.

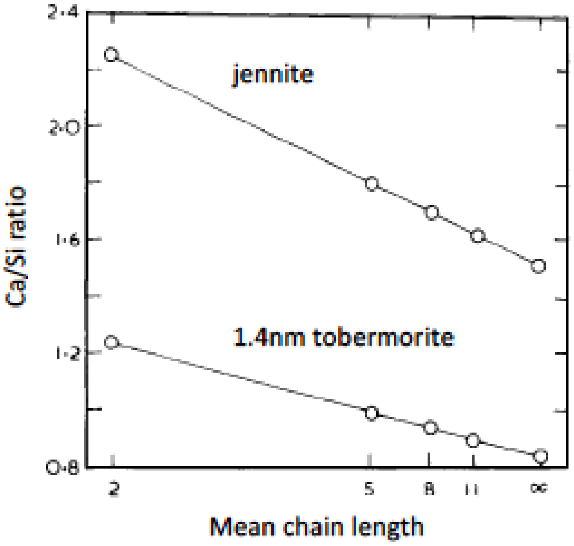

Figure 2.5: Calculated C/S ratio versus chain length for jennite and 1.4nm tobermorite modified by omission of bridging tetrahedra [28].

2.4.3 X-ray Diffraction Analysis

X-ray diffraction analysis is a well established technique for analysis of cement hydration [1]. Cong and Kirkpatrick [7] ran XRD analysis on synthesized C-S-H samples. For samples with C/S ratios above 1.5, CH was present, indicating the C/S ratio naturally occurring C/S of the C-S-H is lower than 1.5. For samples with a C/S ratio of 0.41, amorphous silica was observed, indicating a limit in the amount of silica that can react with the available lime. Cong and Kirkpatrick [7] concluded that most of their samples were semicrytalline with some amount of long-range ordering. Samples showed between 5 and 13 peaks characteristic of C-S-H. The number of peaks decreased with increasing C/S ratio, indicating less long-range order with increasing C/S ratio.

2.5 Compaction and Packing Density

Beaudoin and Feldman [12] compacted the C-S-H they synthesized into discs 31.8 mm in diameter and ∼1.27 mm thick using pressures between 510 MPa and 1360 MPa. Given the relatively high compaction pressures, the densities presented for all the samples were extremely close to one another. Beaudoin and Feldman [12] tested the density of their compacted C-S-H samples using helium pycnometry. Alizadeh and Beaudoin [6] compacted C-S-H samples with C/S ratios of 0.8, 1.0, 1.2, and 1.5 to pressures of 80, 200, 358, and 518 MPa to determine a porosity-pressure relationship for each C/S ratio. Compaction was performed on samples after they had been equilibrated to 11% relative humidity. Porosity was measured using a helium pycnometer to find the solid density, using the apparent volume and the solid volume of the compaction. Jennings [11] modeled C-S-H as a colloid structure, which accounts for the two distinct densities of the C-S-H. The model estimated the density of low-density C-S-H as 1930 kg/m^3 for fully saturated material, and 1440 kg/m^3 for D-dried C-S-H. For the high-density case, saturated density is estimated to be 2130 kg/m^3 and D-dry density as 1750 kg/m^3.

2.6 Effect of Curing at Elevated Temperature and Pressure Conditions

Cement cured under extreme conditions, such as that poured into oil wells and cured while under the high pressure created by the surrounding ocean water, has recently been investigated to gain understanding of how the microstructure, chemical composition, and mechanical properties of cement are impacted by this environment. Le Saout et al. [26, 27] carried out two series of experiments on Class G oilwell cement. In both experiments, samples of cement were cured at 2 conditions: room temperature and atmospheric pressure (T= 293 K and p= 105 Pa), and elevated conditions (T=353 K and p=7e6 Pa). Samples were cured for 30 days. In the first experiment, samples were placed in a brine solution after the initial 30 days for up to 1 year at the two curing conditions listed above. ^{29}Si NMR investigations showed significant differences between the cements cured at each condition both after the initial curing period and after 1 year of leaching. First, the sample cured under atmospheric pressure and temperature showed significant anhydrous cement (Q^0) after the initial 30 day curing phase with only moderate amounts of Q^1 and Q^2 bond, indicating very weak polymerization. In contrast, the sample cured under elevated condition showed Q^1 and Q^2 peaks that were very large compared to the Q^0 peak, with the Q^2 peak being much larger than Q^1. This indicates a much more advanced stage of hydration as well as a much more polymerized C-S-H structure. After 1 year, the relative sizes of Q^0, Q^1, and Q^2 peaks were about equal for the sample cured under normal conditions. It is unclear whether this was caused by an increase in hydration thus lowering the Q^0 peak, an increase in polymerization raising the Q^1 and Q^2 peaks, or a combination of both. The sample cured at elevated conditions showed less change in peaks after 1 year, possibly indicating an increased resistance to leaching. The Q^0 and Q^1 peaks were smaller, while the Q^2 peak appears unchanged. No Q^3 or Q^4 peaks were present in any of the samples. In the second experiment, the class G cement was mixed with silica fume and sand to increase density and, consequently, durability and mechanical properties. Investigation with XRDA and ^{29}Si NMR found that the high pressure/temperature conditions caused CH to be consumed by silica fume to form additional C-S-H. Samples cured under high pressure and temperature showed a shift of the Q^1 and Q^2 connectivities, with a greater proportion of Q^2 connectivities present in the high pressure/temperature samples. This simply means that the C-S-H formed was more polymerized than typical C-S-H.

2.7 Nanoindentation

2.7.1 Surface Preparation

Mondal et al. [29] tried several techniques for polishing hydrated cement surfaces in preparaton for nanoindentation. The first method employed was to use water-based diamond suspensions on texmat pads, spun on an auto-polisher. Gradations down to 0.1 μm were used. The second method used oil-based diamond suspensions of gradations down to 0.1 μm, also on texmat pads spun on an auto-polisher. The third method was to use a dimpler with oil-based diamond suspensions. Finally, the fourth method employed diamond lapping films of gradations down to 0.1 μm on an auto-polisher. SEM images were taken of surfaces obtained after all methods. The diamond lapping films were found to give the smoothest surface, while oil-based diamond suspensions gave the worst surface.

Taking a different approach, Miller et al. [30] prepared hydrated cement samples for nanoindentation by first coarse-grinding the samples to ensure a parallel surface with a 120 grit abrasive paper. Then, using a TexMet P-pad, samples are polished with a 1 μm oil-based diamond suspension. The auto-polisher was spun at 1 cycle per second for 8 hours. After completion, the samples were cleaned in n-decane to prevent any additional hydration. This method was reported to yield good results.

Constantinides and Ulm [31] polished white cement specimens using silicon carbide papers and diamond particles, with the finest stage being 0.25 μm. No additional information was given on this polishing method but nanoindentation results following polishing seemed consistent.

2.7.2 Nanoindentation of Cement and C-S-H

Nanoindentation has become a common method for determining mechanical properties of a material. The benefit of using this technique is that only a small quantity of material is needed for the test, and the test gives better insight into the small-scale material properties rather than the bulk material properties, as is the case with macro-scale testing. The technique employs an indenter tip of known geometry and mechanical properties. The most common tip shapes are a 3-sided pyramidal Berkovich tip and a spherical tip. The tips are typically made of diamond to minimize deformation of the tip during testing.

The book *Nanoindentation* by Fischer-Cripps [32] describes the nanoindentation technique as follows. For the duration of each indentation, the applied load and the displacement of the specimen material are constantly measured, including during unloading. The elastic modulus is extracted by using the top portion of the unloading curve, which is almost purely linear. The top part of the unloading curve is used because it is assumed that there is no reverse plasticity while unloading the sample (see Figure 2.6). That is, all rebound of the material during unloading is assumed to be due purely to elastic deformation and not plastic deformation. The slope of the unloading curve is dP/dh, where P is the load and h is the depth of the indentation. The reduced modulus, E_r is calculated as Eq. (2.3) after Fischer-Cripps [32] :

$$E_r = \frac{1}{2\beta}\frac{\sqrt{\pi}}{\sqrt{A}}\frac{dP}{dh} \tag{2.3}$$

where β is a correction factor to account for the non-symmetrical shape of the indenter tip, which is equal to 1.034 for a Berkovich indenter. A is the contact area of the indenter, which is found by knowing the geometry of the indenter tip as a function of the depth, and the measured depth.

For a Berkovich indenter tip, A is computed by Eq. (2.4) after Fischer-Cripps [32]:

$$A = 3\sqrt{3}h_p^2\,tan^{\,2}\theta \tag{2.4}$$

where h_p is the depth of penetration and θ is the angle the edge of the indenter makes with the vertical (shown in Figure 2.7). The reduced modulus E_r is actually the combined elastic moduli of the material being indented and the indenter tip, which are related by Eq. (2.5) after Fischer-Cripps [32]:

$$\frac{1}{E_r} = \frac{1-\nu^2}{E} + \frac{1-\nu'^{\,2}}{E'} \tag{2.5}$$

where E' and ν' are the elastic modulus and Poisson's ratio of the indenter tip, respectively, and E and ν are the elastic modulus and Poisson's ratio of the indented material, respectively. Given the very high stiffness of the indenter tip material (1220 GPa) compared with the indented material, the reduced modulus is typically used to describe the elastic modulus of the indented material.

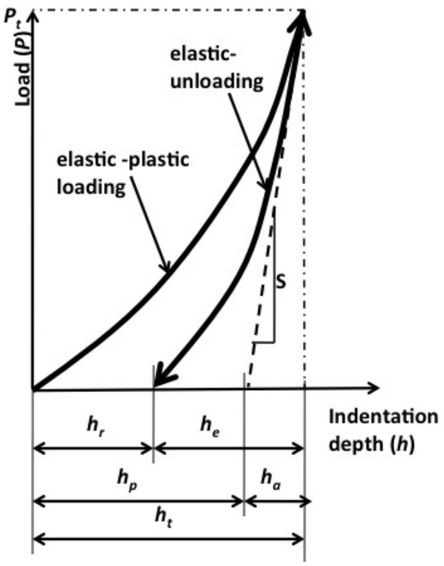

Figure 2.6: Typical load-unload curve for nanoindentation with definitions of terms [32].

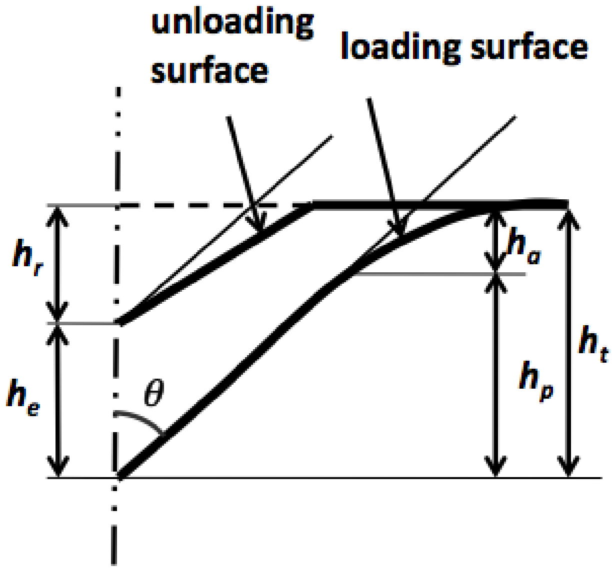

Figure 2.7: Schematic of indentation profile during loading and unloading [32].

In Figure 2.7, h_p is the depth of penetration at load P from the free surface. h_e is the elastically recovered depth after the load is removed. h_r is the residual depth of the impression left by the indenter.

Constantinides and Ulm [31] determined an appropriate depth of indentation for determining properties of C-S-H in hydrated cement. Assuming that the maximum depth of indentation should be 1/10 of the depth of the material phase, the depth range was defined as $\mathrm{d} \ll \mathrm{h}_{max} < \frac{D}{10}$ where d is the size of a single colloidal particle of C-S-H, ~5nm. D is on the order of 1-3 μm, representing the smallest microstructural length scale of cement paste constituents. An appropriate depth range for indentation is therefore selected as $\mathrm{h}_{max} \in [100,300]$ nm. A series of tests was then performed, which determined that a maximum load P_{max}=500μN produces an average maximum indentation depth of h_{max}=167±53nm, within the limits of h_{max}. Multiple indentations were performed on each specimen. For multi-phase materials, a technique for extracting the properties of each phase present is necessary. Constantinides and Ulm [31] showed that the statistical deconvolution technique could be used for separating nanoindentation data into individual phases. This technique will be discussed in detail in section 3.10.

The use of nanoindentation to mechanically characterize hydrated cement has been reported in the past decade. In 2003 and 2004, Constantinides and Ulm [9, 33] used nanoindentation and deconvolution to identify the volume fractions of high-density and low-density C-S-H and their respective elastic modulus and hardness values. This was done by performing 200 indentations on a hydrated, cured Ordinary Portland Cement paste with a 0.5 w/c ratio. The paste was cured for 28 days prior to indentation. It was concluded that a low-density, low-stiffness phase of C-S-H makes up about 67% of the C-S-H present in the paste and has an elastic modulus of 21.7±2.2 GPa. A high-density, high-stiffness phase makes of the remaining 33% of the C-S-H and has an elastic modulus of 29.4±2.4 GPa. Based on their comparison of nanoindentation results with Acker [34], Constantinides and Ulm concluded that these values were characteristic of C-S-H and are not dependent on the overall type of cement, or even the water content. This conclusion came from the fact that Acker's indentation tests were performed on a low w/c Ultra High Performance Concrete (UHPC). According to Acker's tests [34], C-S-H with a C/S ratio of less than 1 has an elastic modulus of 20±2 GPa and C-S-H with a C/S ratio of greater than 1 has an elastic modulus of 31±4 GPa. Hardness values are given as 0.8±0.2 GPa for C/S<1 and 0.9±0.3 GPa for C/S>1. However, no explanation is offered as to how phases were identified, of particular interest is how the C/S ratio of the indented C-S-H phase was measured. This was not explained in the work by Acker [34]. There is also no mention of w/c ratio used, curing time, or sample preparation. In addition, there is no discussion of how many indentations were performed.

Mondal et al. [29] also reported results of hydrated cement indentation and found a value of 23 GPa for elastic modulus of C-S-H in the middle of the matrix, far from unhydrated particles. When indenting C-S-H gel that is close to an unhydrated cement particle, value measured range from 40 GPa to 1.32 GPa.

2.8 Other Mechanical Characterization of Cement and C-S-H

While no work in the literature reported on the nanoindentation of C-S-H, a number of reports provided information on macroscale mechanical properties of C-S-H. Beaudoin and Feldman [12] used a Vickers indenter to determine the microhardness of the compacted C-S-H. They performed all of their tests in a glove box kept at 11% relative humidity. They also used a bending test of compacted discs of synthetic C-S-H to determine its modulus of elasticity. The C-S-H was compacted into discs 31.8 mm in diameter and ~1.27 mm thick using pressures between 510 MPa and 1360 MPa. The modulus of elasticity was determined by measuring the deflection at the center of compacted discs of C-S-H supported at three points. Values for E were never reported, however, a hardness value of H=1337 MPa for C-S-H was provided. The authors concluded that the theoretical zero-porosity E and H values are independent of C/S ratio. It was also suggested that the C-S-H with a C/S ratio of 1.26 has the highest stiffness, which, interestingly, was also the specimens with the highest H/S ratio.

Igarashi et al. [35] also used a Vickers indenter to determine microhardness, but tested cement samples. They made different sample in order to determine the influence of w/c ratio, silica fume, and age on the hardness paste. Type I Portland cement was hydrated with w/c ratios between 0.35 and 0.5. A sample was also made with 10% silica fume at a w/c ratio of 0.4. Samples were cured in water and tested after 14 days and 28 days. Samples were first polished using silicon carbide paper, then loaded under a Vickers indenter at three loads: 0.05 N, 0.15 N, and 0.25 N. 30 indents were performed at each load on each specimen. All tests indicated that microhardness increases with applied load. Tests also showed the sample with silica fume had a lower hardness value than the plain sample at the same w/c ratio. This result could be expected as the silica fume would produce more C-S-H and less CH. C-S-H has a lower stiffness and hardness than CH, so an increase in C-S-H volume fraction would lower the microhardness. However, Igrashi et al. also made standard cylinders to determine the compressive strength, which found a lower strength for the silica fume sample. Compressive strength observations indicated that too much silica fume night have been used, resulting in unreacted silica, which lowered the strength.

Alizadeh and Beaudoin [6] compacted rounded rectangular specimens with dimensions of 12.8mm x 83mm x 0.6-3.0mm thick. Specimens equilibrated to 11%RH were compacted at 496, 517, 331, and 438 MPa for C/S ratios 0.8, 1.0, 1.2, and 1.5, respectively. The specimens were tested using dynamic mechanical analysis (DMA). In this test, the displacement is measured as an oscillating force is applied. The storage modulus E that is obtained is analogous to the modulus of elasticity, E. Elastic modulus values at ∼30% porosity were 23 GPa, 28 GPa, 21 GPa, and 24 GPa for C/S ratios of 0.8, 1.0, 1.2, and 1.5, respectively. When sample porosity increased to 50%, elastic modulus values dropped to 16 GPa, 12 GPa, 8 GPa, and 7 GPa, respectively. Zero-porosity E values were estimated at 231.3 GPa, 132.4 GPa, 94.9 GPa, and 115.1 GPa.

Chapter 3

Experimental Methods

3.1 Experimental Matrix

C-S-H was synthesized and tested as detailed in the experimental matrix shown in Figure 3.1.

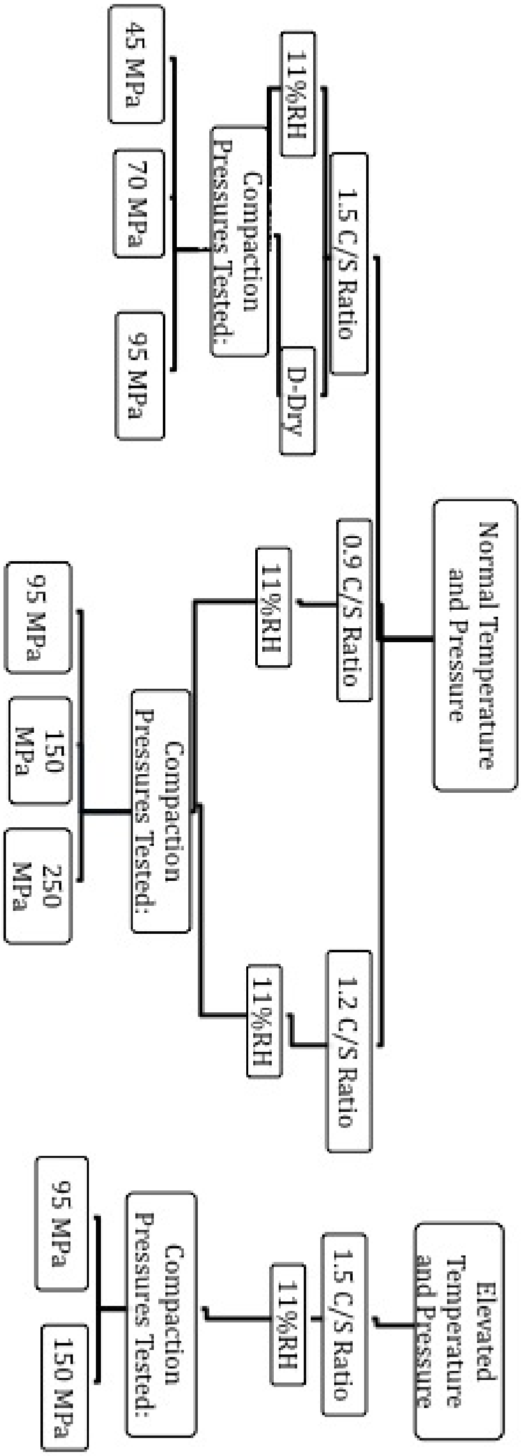

Figure 3.1: Experimental Matrix for C-S-H

3.2 Materials

Reagent grade calcium carbonate ($CaCO_3$) from Mallinckrodt Chemicals was used to make lime (CaO) for the C-S-H. Thermogravimetric analysis (TGA) was run on the $CaCO_3$ to verify its purity, which showed it to be 99.7% pure. Fumed silica from Aldrich with 99.8% purity was used for the silicate portion of the C-S-H, and deionized water was used for all mixing.

3.3 Synthesis of C-S-H– Standard Conditions

C-S-H was synthesized by first calcining $CaCO_3$ into lime (CaO) by heating the $CaCO_3$ to 900°C for 24 hours. Once pure lime was obtained, which was verified by weighing, it was removed from the furnace and placed under nitrogen to prevent carbonation. Then, the lime was mixed with fumed silica at 3 different C/S ratios: 1.5, 1.2, and 0.9, with enough deionized water to make a slurry. These ratios were selected based on past work of other researchers [3, 4, 8, 5, 12]. The slurry was continuously mixed for 7 days to allow complete reaction (Figure 3.2). After mixing, the excess water was filtered off using vacuum. The 1.5 C/S batch was made well before the other two ratios, with two separate batches being made. The two separate batches were dried using two standard methods: D-drying and drying to 11% relative humidity (RH). The goal was to determine the effect of the different water level of the mechanical properties of C-S-H.

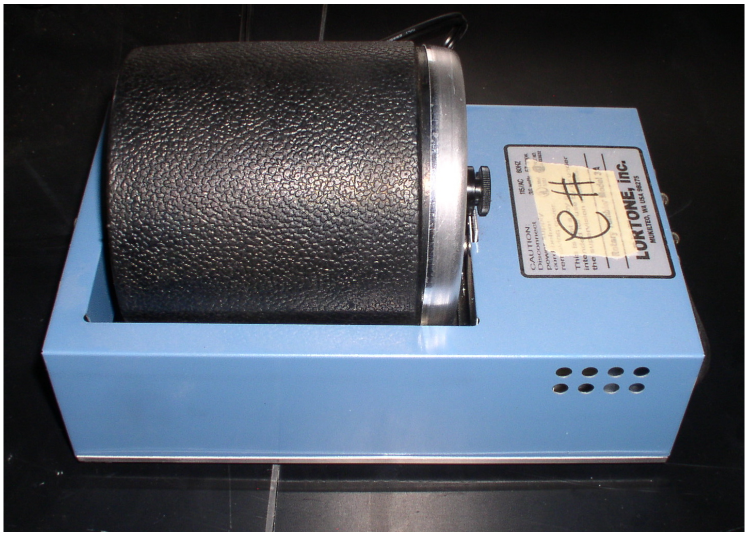

Figure 3.2: Mixer for C-S-H synthesis

The D-drying method was carried out following the procedure described by Copeland and Hayes [15]. Many researchers have used this method to dry cement pastes in the past[14, 36]. The setup consists of a desiccator connected to a glass vacuum trap insulated with corrugated cardboard and a solid rubber membrane (Figure 3.3). The insulated trap is submerged in a bath of dry ice and ethanol, which keeps the trap at -78°C. Water removed from the C-S-H is immediately frozen in the trap. With time, the partial pressure of the ice equalizes with the partial pressure of the water remaining in the C-S-H, creating the end condition. The sample is dried until less than 1 mg of water is lost per 1 g of remaining C-S-H in a 24 hour period. This process took 7-9 weeks typically. The graph of the D-drying results is shown in Figure 3.5.

The second drying method employed was equilibration to 11% RH using saturated lithium chloride (LiCl). This method has been used by many researchers [14, 37, 2]. The salt solution was prepared following ASTM Standard E 104-02 [38]. The system is set up as a series of 3 beakers: the first beaker contains the saturated LiCl solution, which is put on a hot plate on the lowest setting to keep the ambient temperature in the beaker constant. The second beaker contains the C-S-H, and the third contains drierite (calcium sulfate and cobalt chloride) to catch the excess water before it reaches the vacuum pump. This third beaker was connected directly to the vacuum source (see Figure 3.4). The system was first set up without the C-S-H and allowed to reach equilibrium under vacuum for three days. This helps ensure the salt solution is at a steady state. To ensure consistent results, no water was added to the salt solution during or after this initial equilibration period. When the C-S-H was added to its beaker, the hoses connecting the C-S-H beaker to the other 2 beakers were first clamped to keep the state of humidity intact in both. The empty C-S-H beaker was moved to a glove box filled with nitrogen and the C-S-H was added there. The hoses were re-clamped and the beaker reconnected to the rest of the system. A similar clamping procedure was also carried out for the daily weighing of the C-S-H beaker. The C-S-H was dried under this condition until the weight did not change in a 24-hour period. The C-S-H was placed in the system while under a nitrogen environment. This drying process typically took 2 weeks. The 11% RH drying results can also be seen in Figure 3.5. Final percent masses shown on the graph are based on the initial water content of the individual specimens and as such, D-dry and 11% RH values for percent mass remaining cannot and should not be directly compared to one another.

These two standard drying methods were performed to reach a standard water structure given the fact that water is an intrinsic part of the structure. The described procedure is reproducible for the synthesis of C-S-H. D-dry C-S-H has an approximate H/C-S ratio of 0.52 [1], and 11% RH equilibrated C-S-H has an approximate H/C-S ratio of 0.78 [2].

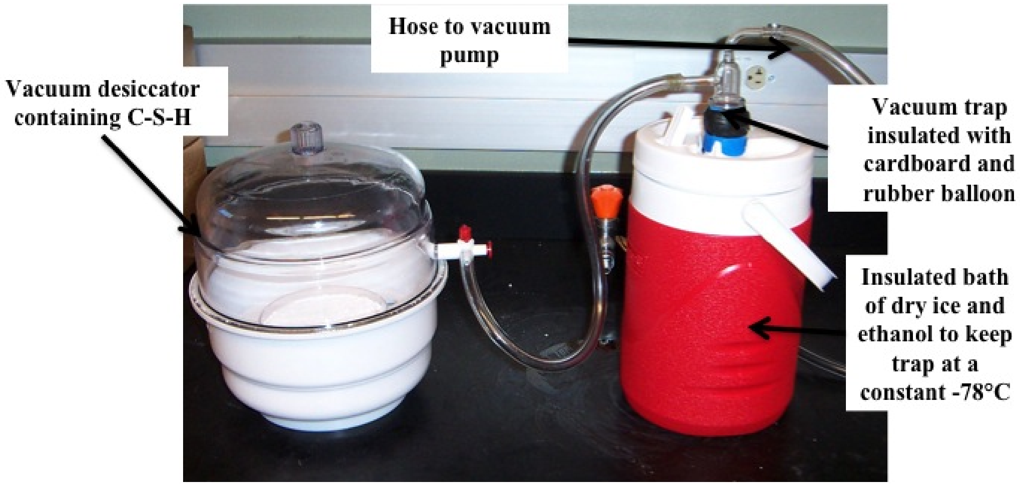

Figure 3.3: Set-up of D-drying method

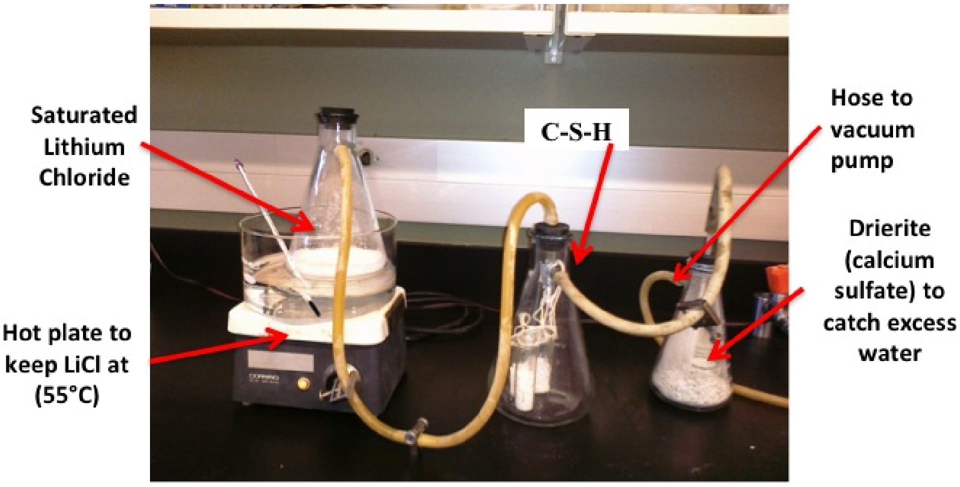

Figure 3.4: Set-up of 11% relative humidity conditioning

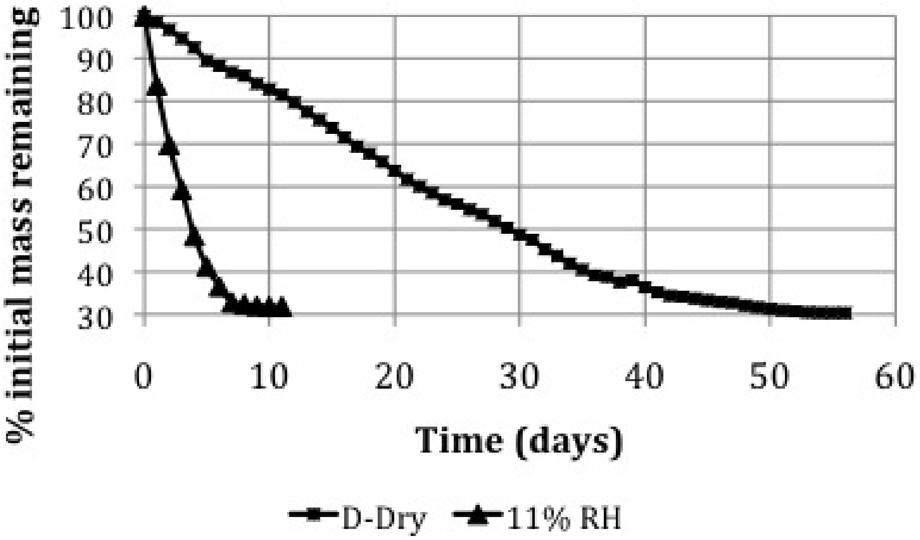

Figure 3.5: 1.5 C/S C-S-H Drying curves. The curve on the left shows the drying results for 11%RH and the right is drying results for D-dry.

It was determined after the mechanical tests on the 1.5 C/S C-S-H that the 11% RH condition gave test results closer to those expected for C-S-H in-situ in cement, and as such the subsequent (0.9 and 1.2 C/S) batches were only dried to 11% RH.

3.3.1 Synthesis of C-S-H– Elevated Conditions

For elevated temperature and pressure a special set-up for the elevated temperature 80°C and pressures 10 MPa (98.7 atm) was prepared as shown in Figure 3.6. A 450 ml Parr pressure vessel was used. Using the heater surrounding the vessel, temperature was elevated and kept constant during the curing time period. To prevent temperature fluctuation in the vessel, 20°C cooling water was circulated through the cooling loop in the vessel. Pressure was applied by injecting nitrogen gas from a compressed nitrogen gas cylinder. The pressure in the vessel was adjusted after the temperature in the vessel stabilized at the design temperature. These conditions were selected to mimic the curing conditions of oil well cement cast-in-place in oil wells [39, 26, 27] The material was continuously mixed for 1 week, after which the excess water was strained off and the material dried to the standard 11% RH condition.

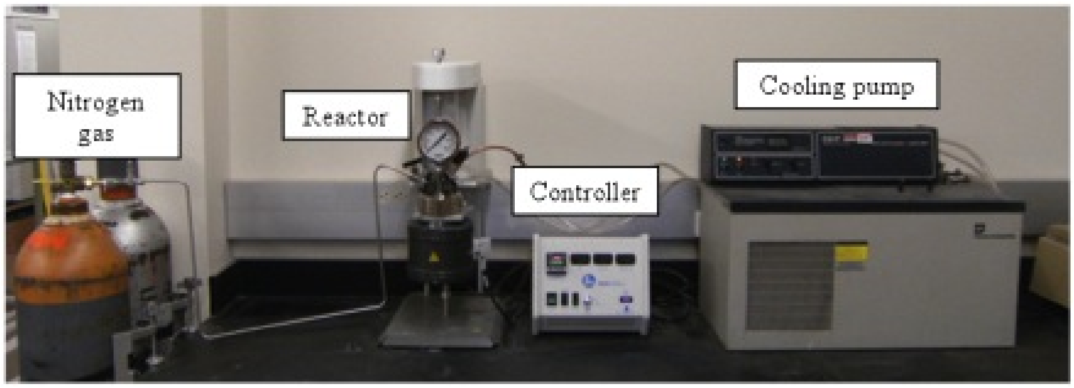

Figure 3.6: Specimen curing set-up to simulate elevated temperature and pressure

3.4 Density

3.4.1 Compaction

All powder preparation was performed in a dry box filled with nitrogen to eliminate any chance of C-S-H contamination (Figure 3.7). The powders were compacted to achieve a range of densities consistent with densities typically observed in ordinary hydrated cement paste. Compaction was performed using a hollow steel cylinder with a 31.75 mm inner diameter, 2 solid steel pistons 31 mm in diameter, 1 steel screen to allow relief of any excess pressure, 1 solid steel disc that fit the cylinder slightly tighter than the pistons to keep material from falling out and to create a smooth surface on one side, and 1 filter paper. ∼4.5 g of powder was used for each compaction, which was placed in the cylinder and steel pistons placed on either side while under nitrogen to avoid specimen contact with CO_2. The load was applied under constant loading rate and held at maximum load for 4 minutes before unloading. The cylinder, pistons, and compression heads of the hydraulic testing machine used are shown in Figure 3.8. A constant load was chosen as opposed to a cyclic, tamping load pattern based on trial-and-error: the resulting C-S-H samples retrieved from cyclic loading were made up of only small chunks. In contrast, when the load applied to the C-S-H was held constant, whole discs of compacted powder were achieved.

Again, the normal 1.5 C/S C-S-H was the first batch to be made, and 10 discs of each type (D-dry and 11% RH) of C-S-H were made using pressures ranging from 25 to 95 MPa. The specimens were extracted from the cylinder under nitrogen (Figure 3.7) and kept there until needed for additional testing. A typical loading-unloading curve for C-S-H is shown in Figure 3.9.

Figure 3.7: Dry box filled with nitrogen to minimize sample contamination

Figure 3.8: Apparatus for compacting discs of C-S-H

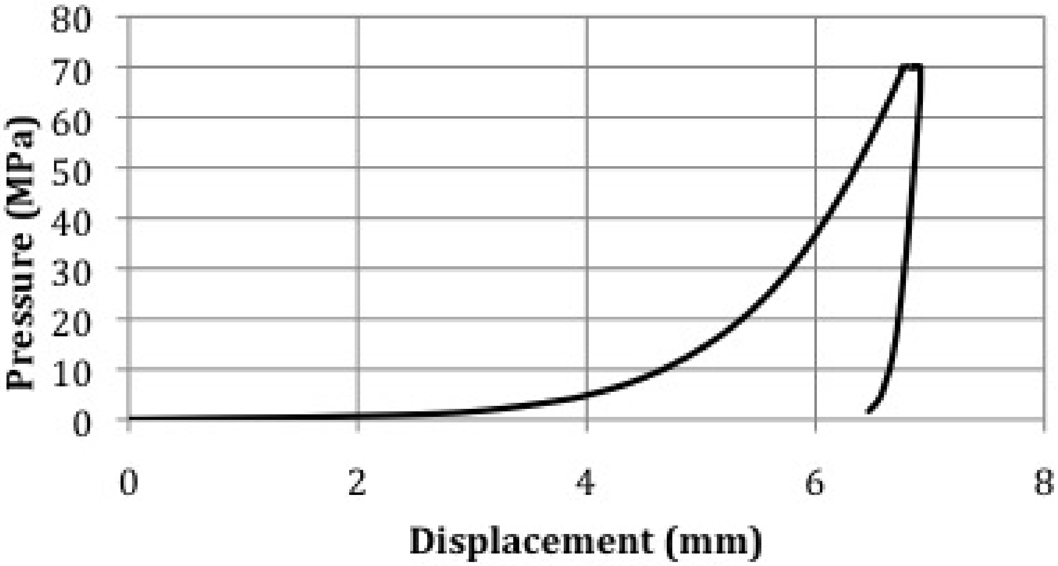

Figure 3.9: Typical Load-Unload curve for C-S-H compaction.

The resultant discs of C-S-H obtained from this compaction procedure are shown in Figure 3.10.

Figure 3.10: Discs of compacted C-S-H.

3.4.2 Density Determination

Density of C-S-H was determined in accordance with ASTM Standard C 914-95 [40]. A Mettler Toledo XS-64 analytical balance with density kit was used in the density determinations (Figure 3.11). Density was determined on 6-8 small pieces produced from the compacted discs. The specimens were first weighed dry and then quickly dipped in paraffin wax conforming to ASTM Standard D 87 repeatedly until the specimens were completely coated. Specimens coated in wax are shown in Figure 3.12. The samples were cooled to room temperature and then re-weighed. Finally, the coated specimens were weighed while submerged in ethanol. Using this mass, the volume of wax can be obtained by knowing the density of the wax (3.1):

$$V_{wax} = \frac{m_{wax}}{\rho_{wax}} \tag{3.1}$$

where m_{wax} is the mass of the wax, which is the difference between the uncoated and coated masses. ρ_{wax} is the density of the wax. While the ASTM Standard calls for water to be used as the submersion fluid, it was observed that air bubbles readily clung to the surface of the wax-coated specimens when submerged in water. It was very difficult if not impossible to remove all of these bubbles from the surface to obtain an accurate reading. In addition, many of the wax-coated samples were less dense than water. This would obviously cause the samples to float, which makes it impossible to measure the mass. Using ethanol as the submersion fluid eliminated these problems. Using the submerged mass, the volume of the entire sample can be found (3.2):

$$V_{ethanoldisplaced} = V_{coatedsample} = \frac{m_{coateddry} - m_{coatedsubmerged}}{\rho_{ethanol}} \tag{3.2}$$

Here, $m_{coateddry}$ is the mass of the sample coated in wax weighed in air, $m_{coatedsubmerged}$ is the mass of the wax-coated sample while submerged in ethanol, and $\rho_{ethanol}$ is the density of the ethanol. Using the result from equations 2 and 3, the volume of the uncoated sample can be calculated (3.3):

$$V_{uncoated} = V_{coatedsample} - V_{wax} \tag{3.3}$$

where $V_{uncoated}$ is the volume of the plain C-S-H sample without wax, $V_{coatedsample}$ is the volume of the C-S-H sample and wax coating combined, and V_{wax} is the volume of the wax coating the C-S-H sample.

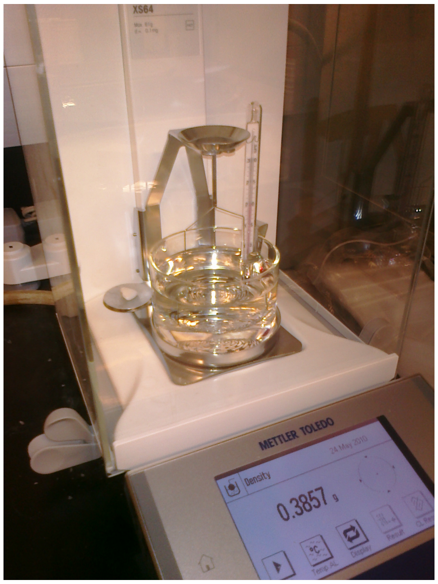

Figure 3.11: Analytical balance used for density measurements

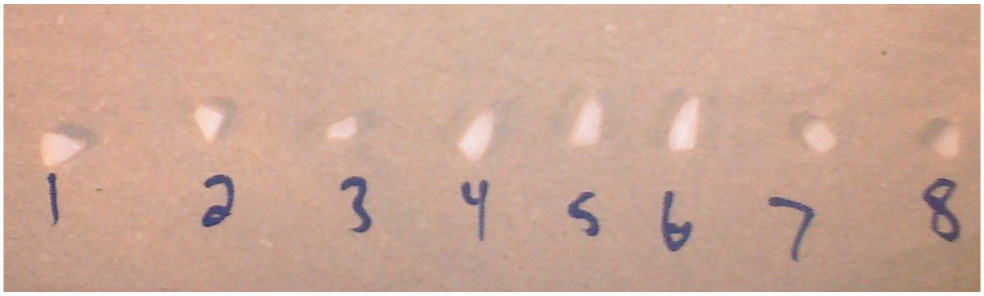

Figure 3.12: C-S-H specimens coated in wax for density measurements.

After many inconsistent test results using the above-described method, it was determined that the wax actually changes density rather significantly day-by-day, even though the wax used was that called for by ASTM. Clearly, the accuracy of the density of wax greatly affects the final results. To solve this problem, the density of the wax was measured at the start of each day of testing. This was done by first measuring the plain, uncoated density of 15 nearly identical coins using the analytical balance. Coins were selected because they are a non-porous material of consistent density whose density results can easily be reproduced. All the coins were coated in wax in the same manner as the C-S-H samples and the densities were retested as described above. All measured values were entered into a spreadsheet, with the density of the wax entered as a variable. Since the coins were the exact same coins in both tests, it is clear that the average density obtained in both test methods should be equal. Using this fact, the Goal Seek function in Microsoft Excel was used to perform iterations on the density of wax until the two average densities for the set of coins were equal. This density was then used for calculations of C-S-H density. It should be noted that the standard deviation for the densities of the wax-coated coins was 10-times that of the standard deviation for the plain coin densities. It is clear that this deviation is a factor of the variation in the wax alone, and not a variation of the uncoated specimens. Therefore, the standard deviations for the C-S-H densities were neglected, as they are not reliable as being a property of the actual wax-free samples. At the end of the day of testing, the wax was stripped from the coins and they were put in an oven at 95°C to remove any residual wax so as not to skew the following days testing. The process was proved accurate enough, and the densities of C-S-H specimens had an average coefficient of variation of 3%.

These experiments, along with published results [41], found that pressures of 95 MPa or higher should be used to produce C-S-H that more closely mimics that of C-S-H found in cement. Thus, the 0.9, 1.2, and elevated 1.5 C/S batches were compacted using just 3 different pressures: 95 MPa, 150 MPa, and 250 MPa.

3.5 Thermogravimetric Analysis

Thermogravimetric analysis (TGA) tests were performed from 25°C to 1000°C, heated at 10°C/min. Shown in Figure 3.13 is the TGA machine used. The TGA test is quite useful for giving calcium hydroxide (CH) and calcium carbonate contents, which are very helpful in determining the purity of C-S-H. While other researchers reported C-S-H content using TGA, the process repeatability seems challenging. This may be attributed to the form of C-S-H analyzed in the literature and examined here. This will be discussed further in Section 5. The temperature ranges presented in the literature considered to be that during which water is lost from C-S-H varies widely among researchers. Odelson et al. [20] reported the range to be between 200°C and 400°C, Alonso and Fernandez [18] determined this range to be 100°C-250°C, Alarcon-Ruiz et al. [19] found the range to be from 180°C-300°C, and Jain and Neithalath [21] used a range from 150°C- 400°C (or the temperature at which water loss from CH begins). We observed a similar temperature range to that reported by Jain and Neithalath [21], as water begins to disassociate from the C-S-H was observed to be between 125°C and 150°C. This starting temperature shift, though small, affected the calculated volume fraction of C-S-H significantly. Negligible mass loss was observed between 350°C and 400°C, so the temperature range considered for C-S-H was capped at 350°C. We suggest the modified equation below to determine C-S-H volume fraction. Eq. (3.4) is a slightly modified version of that suggested by Jain and Neithalath [21]:

$$\%C-S-H = \%ML \times \frac{MW_{C-S-H}}{x \times MW_{H_2O}} \tag{3.4}$$

$\%ML$ is the percentage of mass lost over the temperature range considered to be that during which bonded water from C-S-H is lost. The initial mass is taken as the mass of the sample at 105°C. x can be taken as 2.1 for the 11% RH C-S-H and 1.5 for D-dry C-S-H, as these are the respective moles of water present in each C-S-H. Results from TG analysis will be discussed later.

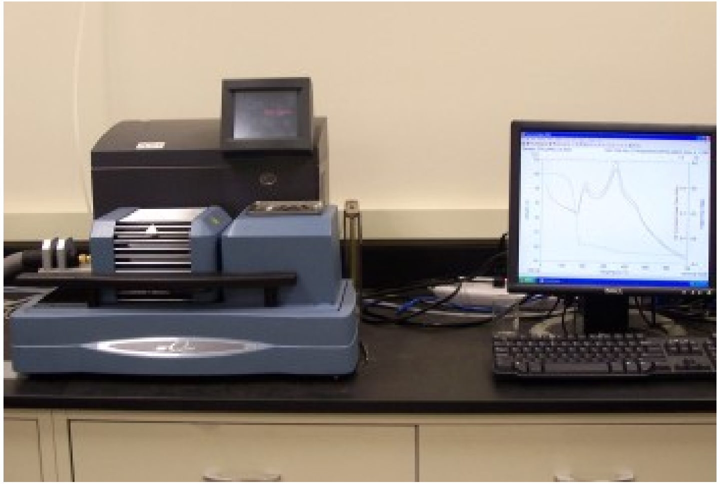

Figure 3.13: Thermogravimetric Analysis Machine

Some testing was performed early on using pieces of the same sample compacted to different pressures to see if there was a correlation between density and thermogravimetric response. As shown in Figure 3.14, however, no correlation was observed. While the samples show varying quantities of water lost, there is no correlation between this and the densities.

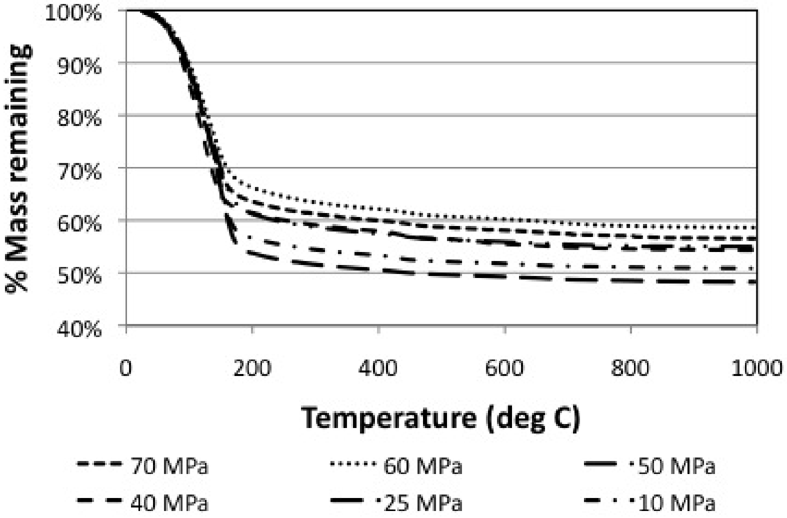

Figure 3.14: TGA response for C-S-H compacted to different densities

3.6 X-ray Diffraction Analysis

X-ray diffraction (XRD) is a long-used method for determining the chemical composition of a material. The pattern given by a particular material is like its fingerprint; it does not change with repeated testing or with different samples of the same material. It is therefore a useful for verifying the formation of C-S-H, as the peaks produced by the samples can be easily compared to peaks found by other researchers, thus confirming or denying the formation of C-S-H, while also being able to see if other compounds exist in the sample, such as CH. All compounds present in an XRD sample will produce their characteristic peaks regardless of other compounds present. XRD analysis was carried out at a scan rate of 1 deg/min from 5 to 70 degree 2θ. Since C-S-H is very amorphous and weakly crystalline, it does not produce strong XRD peaks. As crystalline material has several repeating atomic planes, the angle between the emitted and diffracted X-ray beams is measured. When the X-ray beams having a wavelength λ are emitted with an angle of incidence θ, the beams are diffracted or transmitted according to the distance d between the atomic planes known as basal spacing, which is a specific characteristic of that crystal. Crystallinity is much less prevalent in C-S-H than in a crystalline material such as CH, and as such any CH in the C-S-H sample will show up disproportionately large.

3.7 ^{29}Si MAS-NMR

^{29}Si magic angle spinning nuclear magnetic resonance (MAS-NMR) spectroscopy was performed in 7mm cylinders spun at 4 kHz. Approximately 10,000 scans were performed on each sample. ^{29}Si NMR describes the silicate polymerization of a specimen. Silicate polymerization represents the number of bonds generated by the silicate tetrahedron. A description of silicate tetrahedron having various sharing oxygen is shown in Figure 3.15. A silicate tetrahedron having the number of n

sharing oxygen atoms is expressed as Q^n where n is the number of sharing oxygen atoms ranging from zero to four. As described in Figure 3.15, Q^0 is observed due to unhydrated material, such as remaining tricalcium silicate (C_3S) and dicalcium silicate (C_2S) in cement. Q^1 (end-chain group) and Q^2 and Q^3 (middle-chain group) are typically detected due to the layered structure of C-S-H. Q^4 is the polymerization of quartz and can be observed in silica-rich products such as fly ash and silica fume. For hydrated cement, the most common chain types observed are Q^1 and Q^2 [42]. Q^1 resonates near -79.5 ppm, and Q^2 resonates near -85.3 ppm [7]. Using the intensity fractions of Q^ns, the degree of hydration D_h of a hydrated cement paste can be calculated as Eq. 3.5:

$$D_h = Q^1 + Q^2 + Q^3 \tag{3.5}$$

The degree of polymerization, $\bar{n}$, in the sample is calculated by equation 2.1, repeated here:

$$\bar{n} = \frac{Q^1 + 2Q^2 + 3Q^3}{Q^1 + Q^2 + Q^3} \tag{3.6}$$

Finally, the mean chain length, which is the number of silicates in a connected chain, is calculated by equation 2.2, repeated here: [42]:

$$L = 2 * (1 + \frac{Q^2}{Q^1}) \tag{3.7}$$

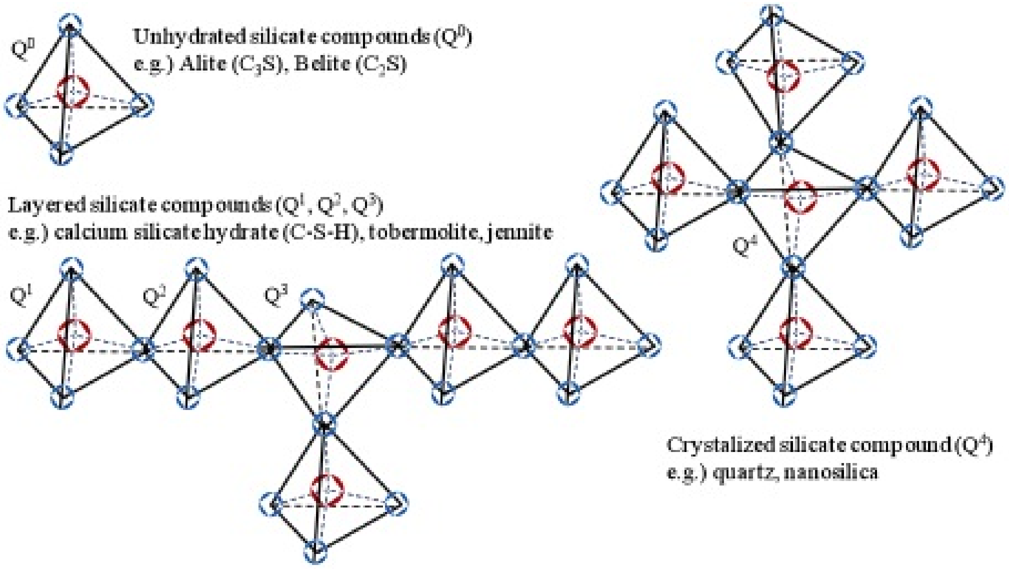

Figure 3.15: Various silicate compounds detectable by ^{29}Si NMR

3.8 Scanning Electron Microscopy

Scanning electron micrographs of C-S-H were taken using a Hitachi S-5200 Scanning Electron Microscope (SEM). Small pieces of compacted C-S-H were placed on the specimen holder arm using double-sided tape. No coating was used or required for imaging. Samples at several densities were viewed, but at the high level of magnification provided by SEM, porosity did not make a difference.

3.9 Nano-Mechanical Characterization

3.9.1 Sample Preparation

Specimens were prepared for nanoindentation by first casting them in a fast-set acrylic to keep the specimens in place for polishing. Specimens are placed in the bottom of a flexible circular mold and acrylic is poured over the top. Sometimes the specimens float up just slightly before the acrylic sets; the coarsest polishing pad (125 micron) is utilized to remove this material to get to a surface of purely C-S-H. The specimens were polished on a Buehler Ecomet 3 polisher with a Buehler Automet 2 power head (Figure 3.16), which applies a constant pressure to the samples and provides additional spin on the samples for increased polishing efficiency. The first method attempted for polishing specimens was as follows. Since the specimens had already been carefully dried to specific water levels, no water was to be used as lubrication for polishing. Again, the normal 1.5 C/S ratio batch was the first batch, and several different polishing techniques had to be employed before a successful method was found. First, as suggested by Miller et al. [30], oil-based diamond suspensions were used. Following polishing with 125-micron, 70-micron, and 30-micron diamond pads, pads saturated with diamond suspensions were employed. A 9-micron oil-based diamond suspension was applied to a Buehler TexMet p-pad, followed by a 1-micron oil-based diamond suspension applied to a Buehler TexMet p-pad. After having adverse results specifically at the 1-micron level, the 1-micron suspension was instead applied to a Buehler TriDent pad, as suggested by the manufacturer. However, both of these pads proved very detrimental to the specimens' smoothness. Using this method, the smoothest the specimens ever got was after polishing with the 30-micron pad. They got progressively worse with subsequent steps. The indentation data retrieved from these samples, consequently, was quite poor.

The fine polishing steps were then changed, using instead diamond lapping films for the 9 and 1-micron stages. The steps used during polishing that were successful were: 10 minutes with a 125-micron diamond pad, 15 minutes with a 70-micron diamond pad, 15 minutes with a 30-micron diamond pad, 30 minutes with a 9-micron diamond lapping film pad, and 1 hour with a 1-micron diamond lapping film pad. In all polishing methods, the pads were lubricated with lapping oil to keep them cool and to disperse removed material. Samples were soniccated in ethanol in between grits. Specimens were exposed to air for the least possible amount of time during the polishing process to avoid C-S-H contamination. During polishing, the sample faces are pressed onto the polishing pad, virtually eliminating exposure to air.

It should be noted that after the specimens were polished, they were left stained by the lapping oil, which was quite obvious as the oil is green and the samples were originally white. A method was not found that could successfully remove the oil without damaging the surface of the specimen. Sonnication in ethanol only removed residual oil sitting on the surface of the specimen, but was ineffective for getting oil out of the pores of the material. It was feared that a harsher chemical such as decane would harm the material and may have even dissolved the acrylic mold that the sample was cast in. In addition, disposal of decane is not as easy as disposal of ethanol. The effect, if any, of the residual oil on the specimens is unknown. However, Miller et al. [30] utilized oil lubrication for cement samples and reported accurate results.

Figure 3.16: Auto-polisher used in preparation of nanoindentation specimens

For the later batches (1.2, 0.9, and elevated 1.5), only the polishing technique using diamond lapping films was employed, which resulted in very smooth surfaces.

3.9.2 Nanoindentation

Nanoindentation was performed using a Berkovich tip loaded at 0.55 mN loading including 0.05 mN preloading. A dwell period of 60 seconds was used at maximum load to account for thermal drift and creep. Thirty points were indented on each specimen in a 3x10 grid, with 50 micron spacing between indents to ensure enough distance between indents as to not affect the results. The results were analyzed to identify the microstructural phases of C-S-H and the mechanical characteristics. For the initial 1.5 C/S material, for both D-dry and 11% RH C-S-H, three disks were tested: 45 MPa, 70 MPa, and 95 MPa. These compact pressures were chosen because they represented a reasonable spread of densities for C-S-H given the density observations reported earlier. For the 0.9, 1.2 , and elevated 1.5 C/S batches, discs compacted at 95 MPa, 150 MPa, and 250 MPa were tested. A typical nanoindentation curve is shown in Figure 3.17. The horizontal dashed line in the figure is the level of preloading applied to the specimen to ensure contact prior to testing.

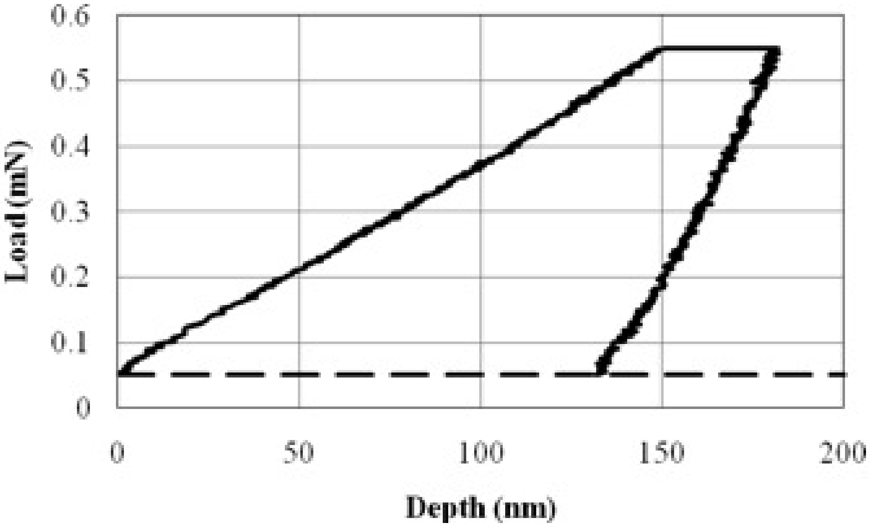

Figure 3.17: Typical nanoindentation curve of C-S-H

The elastic modulus is extracted by using the top portion of the unloading curve, which is almost purely linear. The top part of the unloading curve is used because it is assumed that there is no reverse plasticity while unloading the sample. That is, all rebound of the material during unloading is assumed to be due purely to elastic deformation and not plastic deformation. The slope of the unloading curve is dP/dh, where P is the load and h is the depth of the indentation. The reduced modulus, E_r is calculated as (3.8) [32] :

$$E_r = \frac{1}{2\beta}\frac{\sqrt{\pi}}{\sqrt{A}}\frac{dP}{dh} \tag{3.8}$$

where β is a correction factor to account for the non-symmetrical shape of the indenter tip, which is equal to 1.034 for a Berkovich indenter. A is the contact area of the indenter, which is found by knowing the geometry of the indenter tip as a function of the depth, and the measured depth. For a Berkovich indenter tip, A is computed by Eq. (3.9) [32]:

$$A = 3\sqrt{3}h_p^2 tan^2\theta \tag{3.9}$$

where h_p is the depth of penetration and θ is the angle the edge of the indenter makes with the vertical. The reduced modulus E_r is actually the combined elastic moduli of the material being indented and the indenter tip, which are related by Eq. (3.10) [32]]:

$$\frac{1}{E_r} = \frac{1-\nu^2}{E} + \frac{1-\nu'^2}{E'} \tag{3.10}$$

where E' and ν' are the elastic modulus and Poissons ratio of the indenter tip, respectively, and E and ν are the elastic modulus and Poissons ratio of the indented material, respectively.

3.10 Statistical Deconvolution Analysis

Nanoindentation and ^{29}Si MAS-NMR results were analyzed using the statistical deconvolution analysis technique [31]. The objective of statistical deconvolution is to estimate the volume fraction of the different phases in C-S-H in nanoindentation and their respective properties, or the fraction of a specimens silicon bonds with a certain level of polymerization in NMR. For the statistical deconvolution of experimental results, frequency density functions of nanoindentation results and NMR spectra are assumed as a combination of the number of n normal distributions such as in Eq. (3.11):

$$p(x_j) = \alpha \sum_{i=1}^{n} f_i \frac{1}{\sigma\sqrt{2\pi}} e^{-\frac{(x-\mu)^2}{2\times\sigma_i^2}*f_i} \tag{3.11}$$

Here, α is scale factor, which can be the number of nanoindentation tests for the frequency density function or the maximum intensity for NMR spectra. n can be considered as the number of different phases characterized by the property x on abscissa (either elastic modulus or ppm for nanoindentation and NMR, respectively). f_i, σ_i and μ_i represent the volume/surface fraction occupied by the i-th phase, the standard deviation, and the mean values of the i-th phase respectively. The convolution function in Eq. (3.11) is determined by minimizing the standard error with the experimental observations. This can be done by maximizing the *R-squared* value computed as in Eq. (3.12):

$$R^2 = 1 - \sum_{j=1}^{m} [y(x_j) - p(x_j)]^2 \tag{3.12}$$

where x_j and $y(x_j)$ are the j-th abscissa and ordinate values of the experimental results respectively and m is the number of the experimental results. For nanoindentation results, m is equal to the number of bins used to construct of the frequency density function. To properly fit the convolution function to the experimental results, the *R-squared* value needs to be maximized (close to 1). The mean, standard deviation, and volume fraction values of the n phases are all unknowns. The sum of all the volume fractions is equal to 1, and $3n$-1 unknowns of the convolution function need to be determined. The number of bins needed to construct the frequency density function should be larger than $3n$-1. An example of deconvolution is shown in Figure 3.18. The circles represent the actual experimental data, and the solid black line is the combination of all the individual PDFs. The solid theoretical PDF line should match as closely as possible with the experimental data points for successful deconvolution.

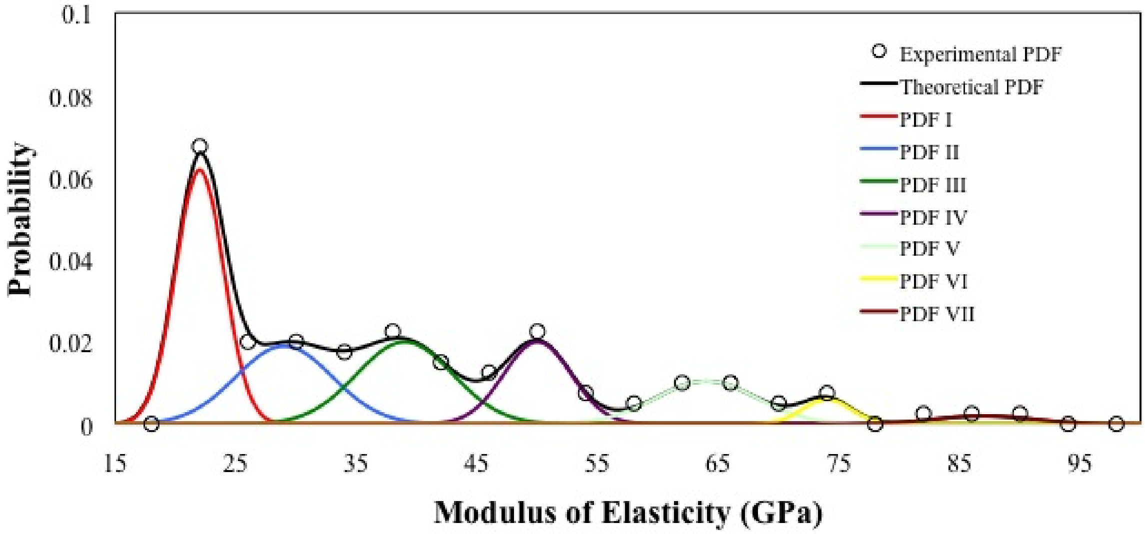

Figure 3.18: Example of deconvolution

Chapter 4

Results and Discussion

4.1 1.5 C/S C-S-H

The density versus pressure curves for 1.5 C/S C-S-H dried to 11%RH and D-dry conditions are shown in Figure 4.1.

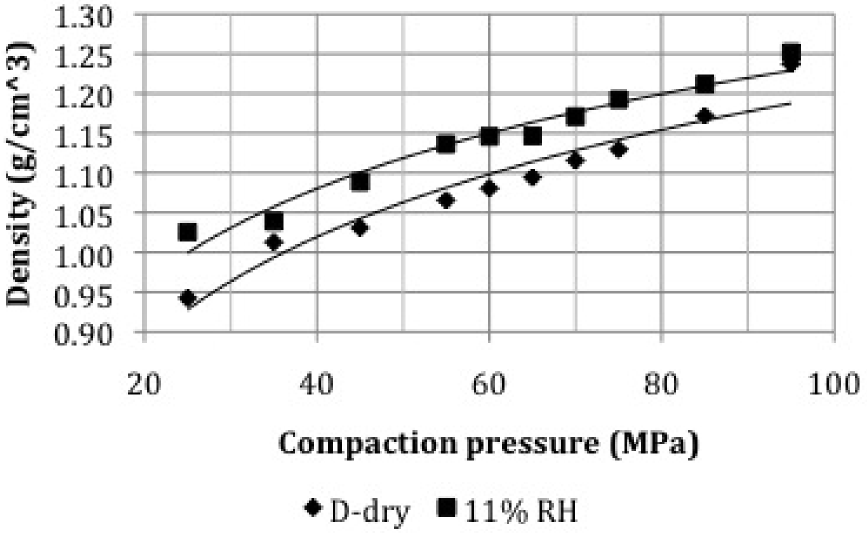

Figure 4.1: Compaction pressure versus density curve of 1.5 C/S C-S-H and 11%RH and D-dry states

Density measurements show that given equal compacting pressures, D-dry samples compact to a lower density than 11%RH samples. D-dry samples have a lower moisture content than the 11%RH samples, equivalent to about 7% humidity. Moisture aids in the attraction or sliding of C-S-H sheets with one another, so it is reasonable to assume that increased water content of 11% RH specimens would help the powders compact tighter than D-dry ones.

TGA curves for 1.5 C/S C-S-H are shown in Figure 4.32. The pore structure of C-S-H in situ in cement is inherently different than that of synthetic C-S-H. For instance, the C-S-H in hydrated cement is constrained during hydration due to the surrounding cement paste. The synthetic C-S-H is hydrated while in suspension, so it is free to form an entirely different pore structure. In addition, the synthetic C-S-H is dried, as described earlier, before being compacted to densities similar to that of cement. This is very important, as much of the water considered to be part of the structure is interlayer or pore water, not chemically bound water as in the case of CH. For example, specimens tested with TGA by Jain and Neithalath [21] were of a hydrated cement paste, not of synthetic C-S-H. The pore structure and consequently the path the water must take to escape the specimen can be quite different between a cement paste and synthetic C-S-H, and as such it is not possible to directly compare side-by-side the portion of a TGA of C-S-H in situ in cement and that of synthetic C-S-H. The results obtained in this study indicate 92.0% C-S-H in the 11% RH specimens, with the balance being composed of 6% CH and 2% $CaCO_3$. D-dry specimens indicate 81.5% C-S-H with the balance made up of 13.6% CH and 4.9% $CaCO_3$.

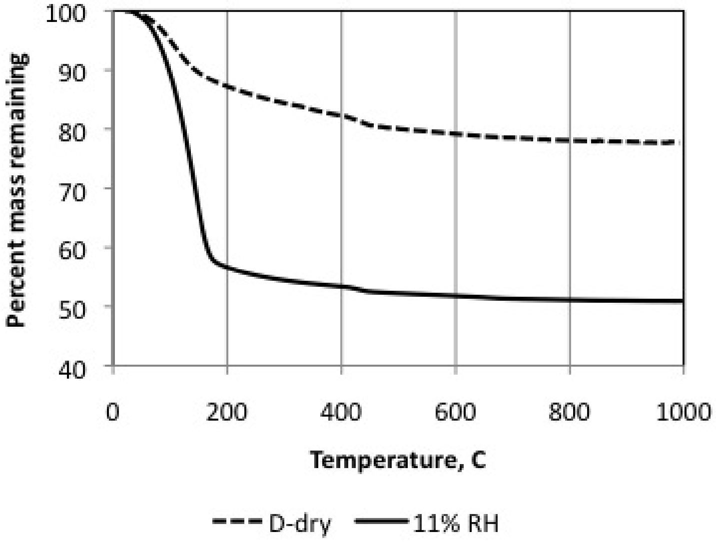

Figure 4.2: TGA Curves. The top curve is representative of D-dry and the bottom 11%RH.

The XRD analysis of the D-dry C-S-H showed several phases of C-S-H as well as some CH and $CaCO_3$ as shown in Figure 4.3. XRDA on the 11% RH C-S-H showed several phases of C-S-H mixed with some CH, also shown in Figure 4.3. As discussed in section 3.6, CH peaks show up disproportionately high for their actual volume in the sample, since CH is much more crystalline than C-S-H and XRD peaks are produced by x-ray beams diffracting off crystals. For both types of C-S-H, the XRD peaks attributable to C-S-H lined up well with published results [5, 7]. XRD analysis on the 1.5 C/S 11%RH C-S-H showed several phases of C-S-H mixed in with some CH, as shown in Figure 4.3 as well. Peaks present at 29°, 32°, 7°, and 48° are characteristic of C-S-H. The slim peaks present at 18° and 34° indicate CH present in the sample. It is nearly impossible to determine if any $CaCO_3$ is present, as the strongest peak would appear around 29.5°, coincident with peaks for C-S-H. The other peaks representative of $CaCO^3$ are so weak that they could easily be lost in the background noise of the spectra.

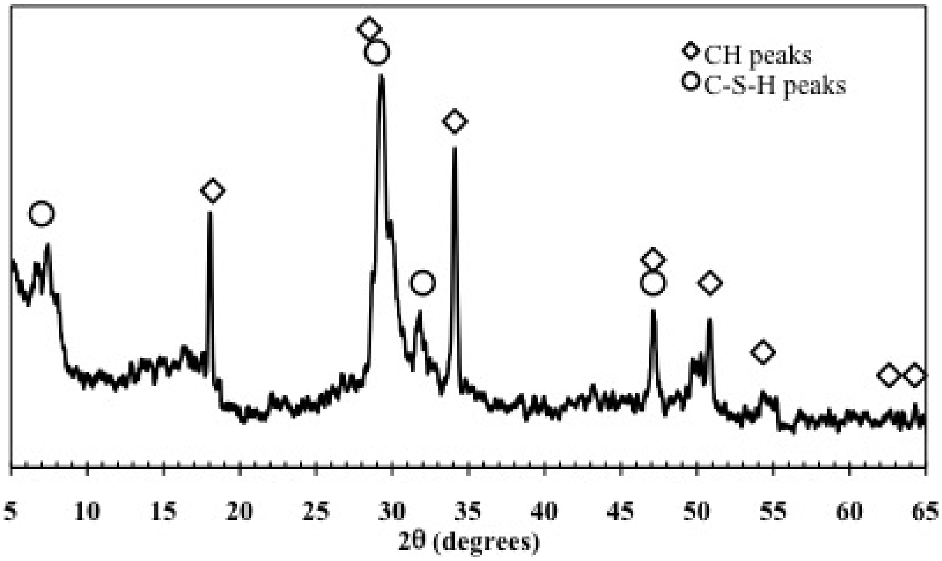

Figure 4.3: XRDA Plot of 1.5 C/S C-S-H.

NMR spectra of D-dry and 11%RH C-S-H with C/S ratio of 1.5 are shown in Fig. 4.4. Statistical deconvolution analysis was performed on NMR results, indicating 74% Q^1 and 26% Q^2. ^{29}Si MAS NMR results showed near-identical peaks for both the 11%RH and D-dry specimens, which is expected since both types have identical C/S ratio and were hydrated using the same method, and since silicon bond is not dependent on water content. The results observed match well with data in the literature [18, 7, 42, 24, 43, 25]. The majority of silicate bonding is Q^1, with a noticeable but smaller peak of Q^2 sites. NMR spectra of both types of C-S-H are shown in Fig. 4.4. Statistical deconvolution of the peaks showed 74% Q^1 and 26% Q^2. The results of statistical deconvolution for the volume fraction of Q^1 and Q^2 is similar to that reported recently by Beaudoin et al. [25], who reported 80.6% Q^1 and 19.4% Q^2. The findings from the ^{29}Si NMR also show that the material is fully hydrated. Unhydrated material would show as a Q^0 peak around 74 ppm, which is not present. The degree of polymerization $\bar{n}$ and mean chain length L for 1.5 C/S at D-dry and 11%RH are shown in Table 4.1, calculated using equations 2.1 and

2.2. Chain lengths observed are not similar at all to either jennite or tobermorite. Jennite is reported to have an almost infinite chain length at a C/S ratio of 1.5, while tobermorite does not form chains at such a high C/S ratio [28].

Table 4.1: Polymerization and Chain Length for 1.5 C/S C-S-H

	11%RH	**D-dry**
Degree of polymerization	1.261	1.264
Mean chain length	2.71	2.72

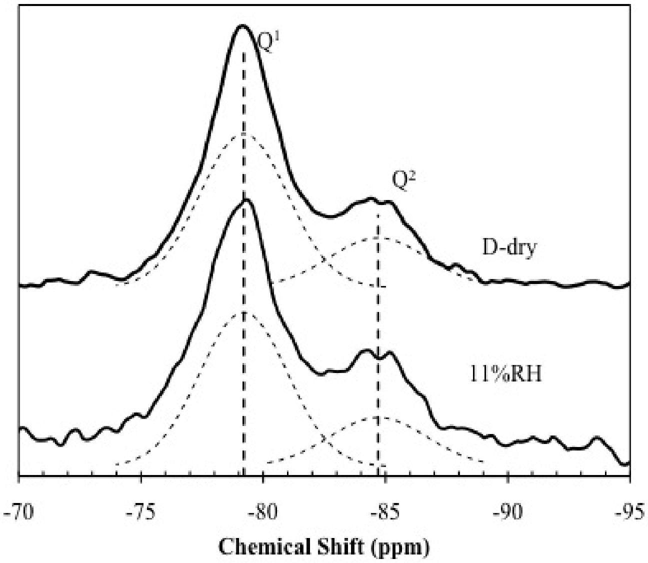

Figure 4.4: ^{29}Si NMR Spectra of 1.5 C/S C-S-H at D-dry and 11%RH conditions. Deconvolution of the peaks showed 74% Q^1 and 26% Q^2.

The investigation of both C-S-H powders showed a relatively homogenous C-S-H with CH present only in very rare occasions. SEM images are shown in Figures 4.5, 4.6, and 4.7.

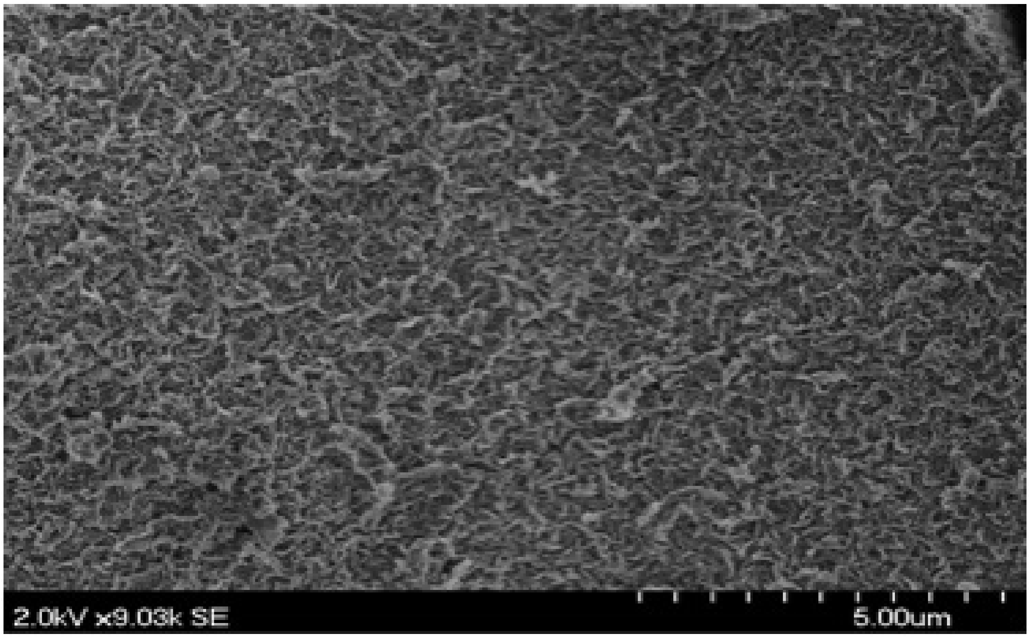

Figure 4.5: SEM Micrograph of Synthesized C-S-H at 9000 times zoom

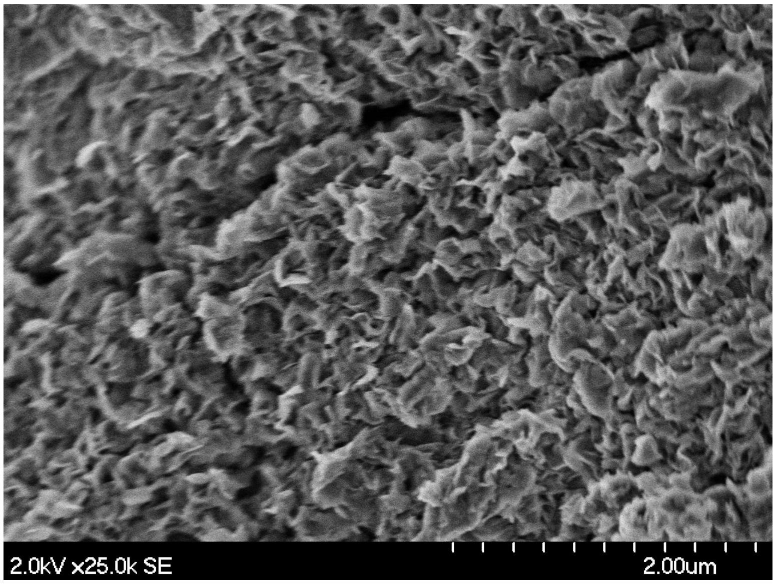

Figure 4.6: SEM Micrograph of Synthesized C-S-H at 25,000 times zoom

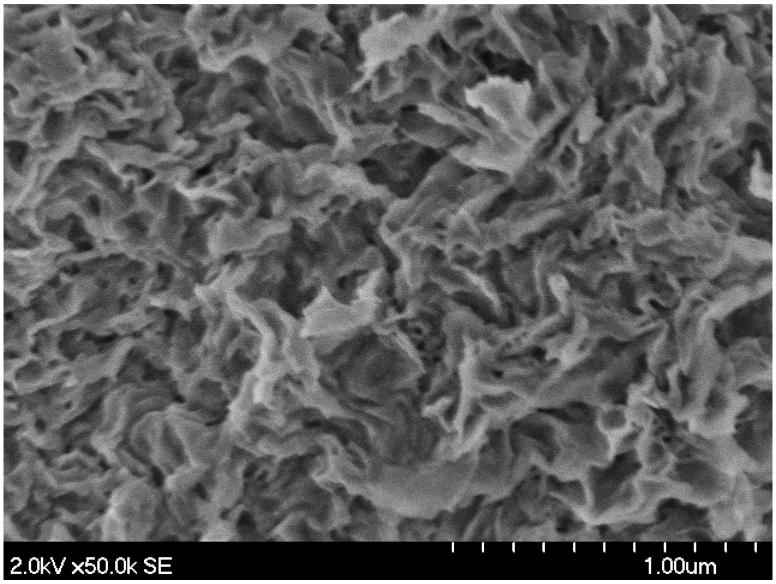

Figure 4.7: SEM Micrograph of Synthesized C-S-H at 50,000 times zoom

Nano-indentation results show an obvious increase in elastic modulus with increasing density for both 11% RH and D-dry specimens. It is observed that as compaction pressure increases, the discrepancy between 11% RH and D-dry Youngs modulus of elasticity observations increase, with the D-dry value dropping to a value lower than expected for C-S-H. This difference may be attributed to the difference in moisture contents of both types of C-S-H. The lower moisture content in D-dry C-S-H seems to be the only factor contributing to this lower stiffness, as all other parameters (curing, C/S ratio, compaction technique) are similar for both types of C-S-H. This difference between values is likely to keep increasing with greater pressures because the D-dry C-S-H lacks the moisture to hold together for high densities. These results are presented in Figure 4.8 and Table 4.9. Points shown in Figure 4.8 are the elastic moduli for each individual identified phase, sized relative to their relative surface fraction.

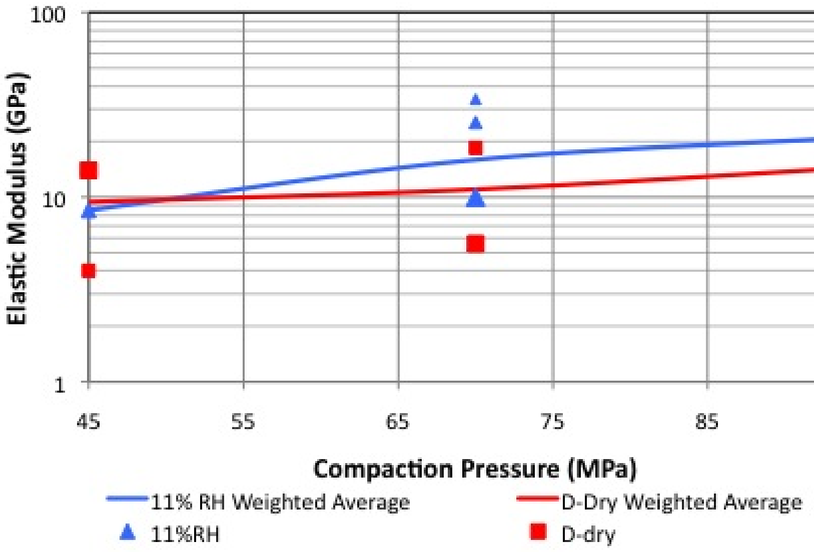

Figure 4.8: Elastic modulus versus compaction pressure for C-S-H.

Table 4.2: Surface fractions and Young's modulus for 11%RH and D-dry 1.5 C/S C-S-H

Compaction Pressure	CSH Phase Categorization	11%RH		D-Dry	
		Surface Fraction	Young's Modulus (GPa)	Surface Fraction	Young's Modulus (GPa)
45 MPa	VLD LD	100% 0.0%	8.5 ± 2.5 N/A	46.0% 54.0%	4.0 ± 3.1 14.0±4.2
70 MPa	VLD LD HD	69.0% 17.0% 14.0%	10.0±3.7 25.4 ± 2.8 34.0 ± 1.7	58.0% 42.0% 0.0%	5.6 ± 4.6 18.5±6.9 N/A
95 MPa	VLD LD HD	22.0% 0.0% 78.0%	6.0 ± 4.8 N/A 25.4 ± 6.6	27.0% 73.0% 0.0%	5.8 ± 4.4 17.8 ± 7.0 N/A

The deconvolutions of elastic modulus for D-dry C-S-H are shown in Figures 4.9-4.11. The specimen compacted to 95 MPa shows 4 values: 5.8, 17.8, 37.0, and 57.0 GPa (Figure 4.11). However, given the fact that TG analysis showed fractions of the specimen to be CH and $CaCO_3$, and knowing the approximate elastic moduli of these phases, 2 phases were identified to be CH and $CaCO_3$. The majority of the sample is observed to have 17.8 GPa. According to Contantinides and Ulms classifications [9], all the C-S-H at this compaction and dryness level is classified as low density (LD) or very low density (VLD) C-S-H. VLD C-S-H is of course possible to create synthetically, but is not typically observed within cement paste. The weighted average for the 95 MPa sample is 14.56 GPa, which classifies it as VLD. However, it is important to note that specimens indented in the literature were of hydrated cement that were not subjected to any drying other than being in air during preparation for and undergoing indentation. [9, 34, 29]. The 11%RH C-S-H sample compacted to 95 MPa showed 3 elastic modulus values: 6.0, 25.0, and 45.0 GPa. However, from knowledge of the properties of CH and TG results showing some CH content, the 45 GPa phase is believed to be due to CH and is neglected in calculations of C-S-H properties. The weighted average of the samples elastic modulus was 21.132 GPa, which is slightly low but still in line with published elastic modulus values, putting it into the category of low density (LD) C-S-H. It seems that the results of the C-S-H dried to 11%RH are closer to those produced in well-cured cement specimens, which is most likely due to the increased water content of the 11%RH specimens over the D-dry specimens.

Samples from both batches compacted to 45 MPa gave very similar elastic modulus results, with an average value around 9 GPa (Figures 4.9 and 4.12). It is obvious that this compaction level is too low to produce a C-S-H with density mimicking that of in-situ C-S-H. At this compaction level, the water content does not appear to come into play in determining elastic modulus, as the low density seems to be the controlling factor in this case. 70 MPa also appears to be too low of a pressure to produce a C-S-H sample mimicking in-situ C-S-H (Figures 4.10 and 4.13). The weighted averages of elastic modulus for 11%RH and D-dry compacted at 70 MPa were 15.98 and 12.98 GPa, respectively.

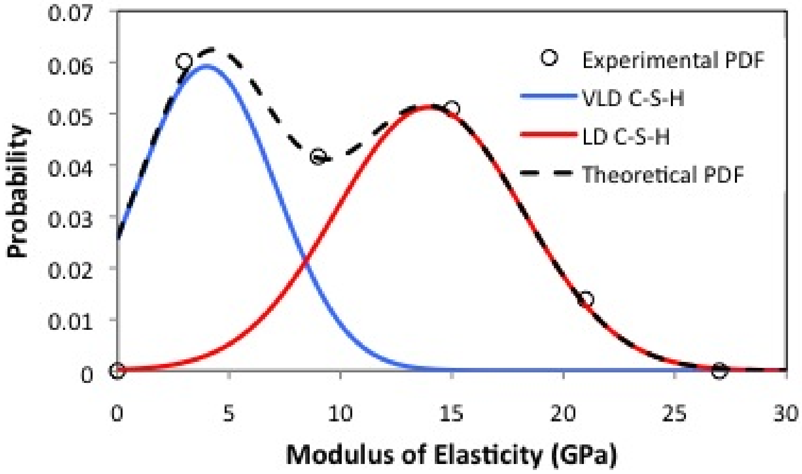

Figure 4.9: Deconvolution of D-dry 1.5 C/S C-S-H compacted to 45 MPa

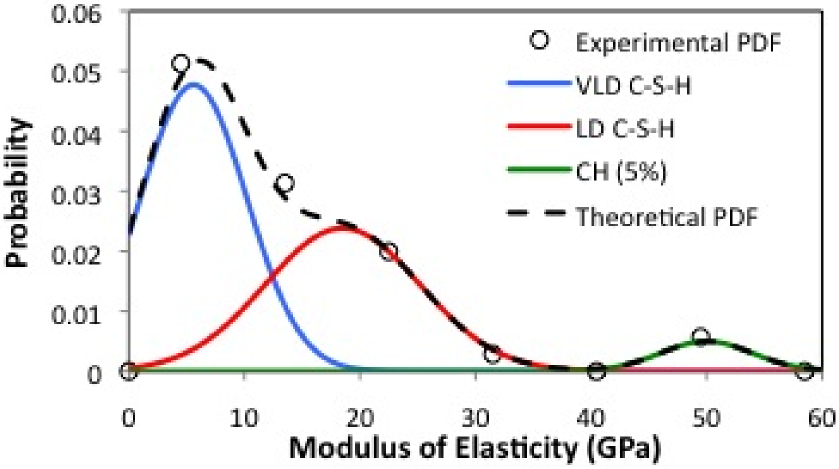

Figure 4.10: Deconvolution of D-dry 1.5 C/S C-S-H compacted to 70 MPa

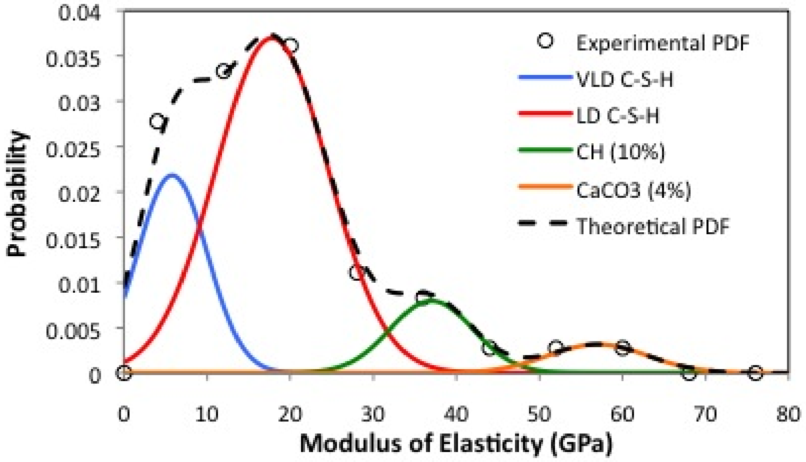

Figure 4.11: Deconvolution of D-dry 1.5 C/S C-S-H compacted to 95 MPa

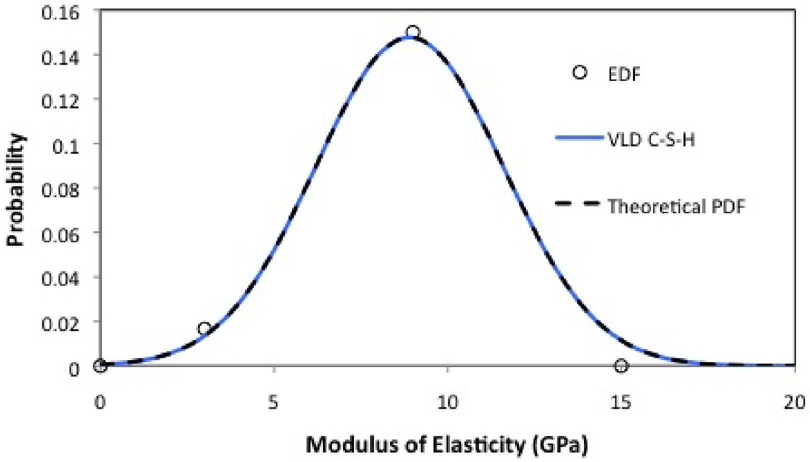

Figure 4.12: Deconvolution of 11%RH 1.5 C/S C-S-H compacted to 45 MPa

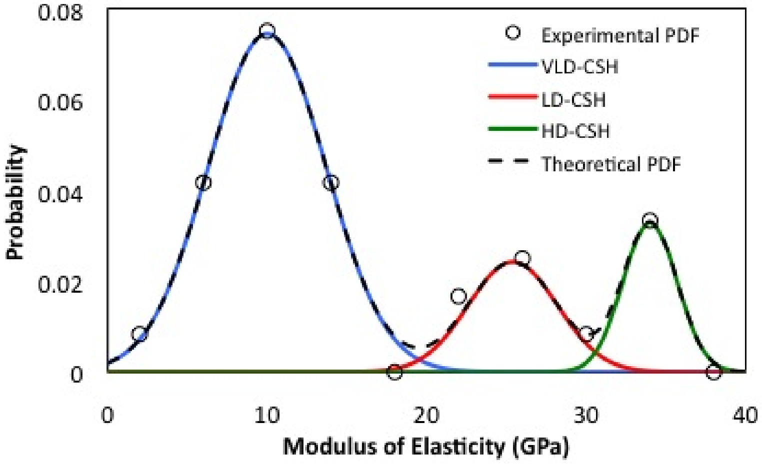

Figure 4.13: Deconvolution of 11%RH 1.5 C/S C-S-H compacted to 70 MPa

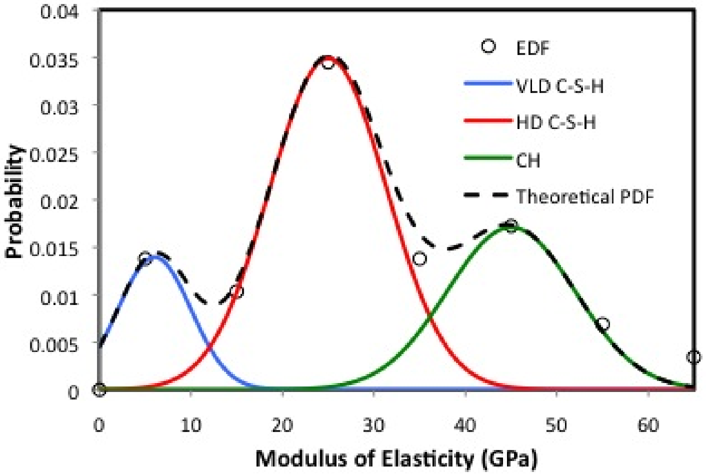

Figure 4.14: Deconvolution of 11%RH 1.5 C/S C-S-H compacted at 95 MPa

4.2 0.9 and 1.2 C/S C-S-H

The density versus pressure curves for 1.2 and 0.9 C/S C-S-H dried to 11%RH are shown in Figure 4.15. Given equal pressures, the 1.2 C/S C-S-H was observed to be the most dense. Both the 0.9 and 1.2 C/S material densities were greater than that of the 1.5 C/S C-S-H compacted at the same pressure, shown in Figure 4.15 for comparison. These densities are more similar to those published by Jennings [11] and Constantinides and Ulm [31] as discussed in section 2.5. It is important to note that the 1.5 C/S ratio C-S-H was compacted up to 95 MPa only. There is not a clear explanation on the reduction of densities for the 0.9 C/S C-S-H ratio compared to the 1.2 C/S ratio.

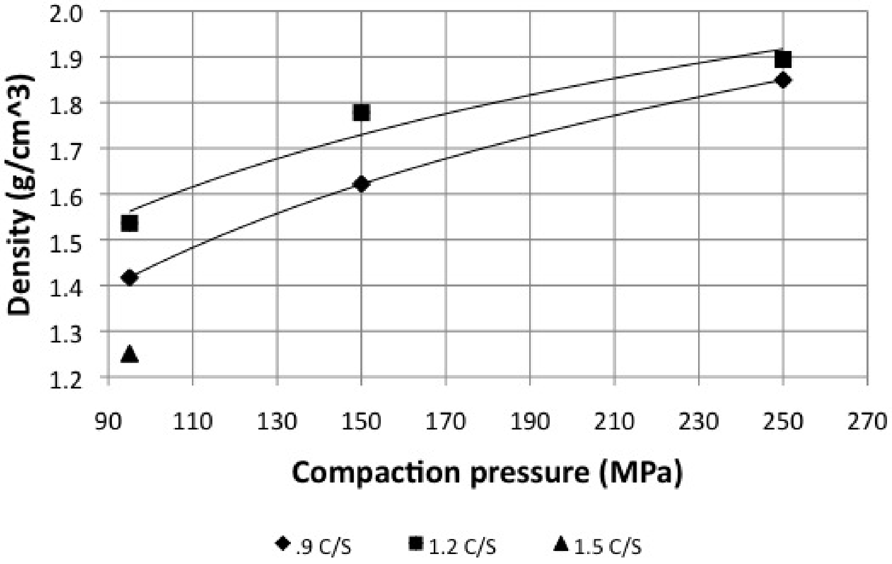

Figure 4.15: Compaction pressure versus density curve for C-S-H at 0.9 and 1.2 C/S ratios

XRD analysis of C-S-H made at 0.9 and 1.2 C/S ratios showed only peaks for C-S-H with no CH present (Figures 4.16 and 4.17). Peaks observed match well with published results for C-S-H [5, 7, 42], helping to prove the formation of C-S-H. If any

$CaCO_3$ is present, its signal is too weak to be seen over the background noise of the spectra. The strongest peak would appear around 29.5°, coincident with the broad C-S-H peak present.

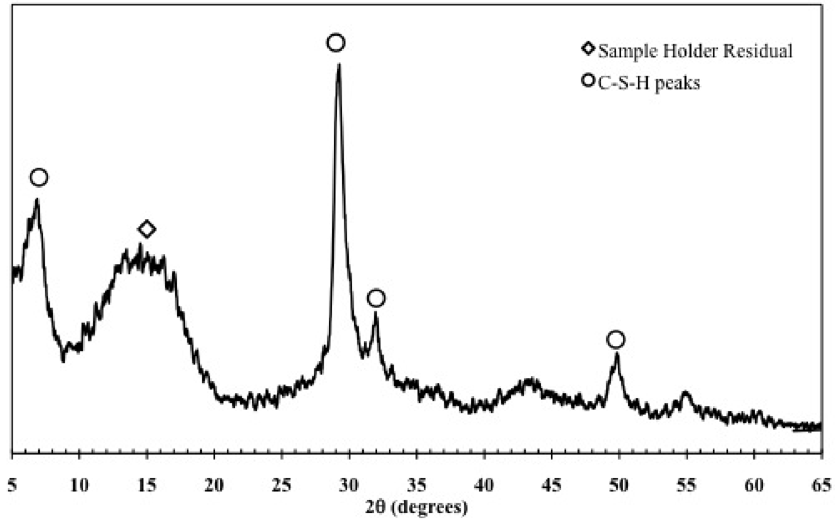

Figure 4.16: XRDA Plot of 0.9 C/S C-S-H.

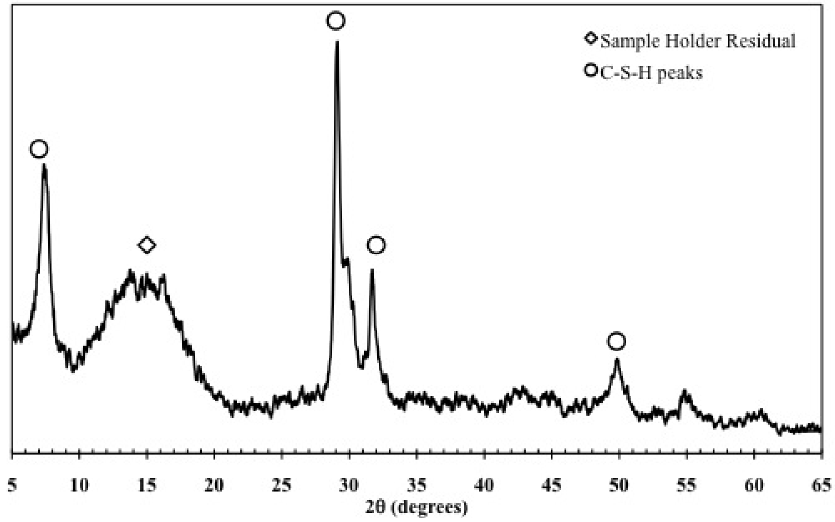

Figure 4.17: XRDA Plot of 1.2 C/S C-S-H.

NMR Spectra are compared with each other and with the 1.5 C/S C-S-H synthesized earlier for comparison (Figure 4.18). As C/S ratio decreases, a clear shift in the Q^2/Q^1 ratio is observed, as seen in Table 4.3 and Figure 4.18. Only a slight change in the Q^2/Q^1 ratio is observed between 1.5 C/S and 1.2 C/S; however, a very substantial increase in polymerization of the silica, indicated by an increase of Q^2 bonding, is seen when the C/S ratio drops to 0.9. These results are similar to those observed by other researchers [7, 42] and further prove the formation of C-S-H. The shift in Q^2 is substantial and might require further repetition of the experiments. However, they align well with published results [25]. The degree of polymerization $\bar{n}$ and mean chain length for 0.9 and 1.2 C/S are shown in Table 4.4, calculated using equations 2.1 and 2.2. As a reference for scale, the maximum polymerization, 100% Q^3 bond, would have a polymerization value of 3. 100% Q^1 bond would have a polymerization value of 1. Chain lengths observed are not similar at all to jennite, but are somewhat similar to lengths reported for tobermorite. Jennite is reported to have an almost infinite chain length at C/S ratios of 1.2 and 0.9, while tobermorite has chain lengths of 2.3 and 11 for 1.2 and 0.9 C/S ratios, respectively [28].

Table 4.3: Q^1 and Q^2 volume fractions of C-S-H

C/S	**Q^1**	**Q^2**	**Q^2/Q^1**
1.5	0.738	0.262	0.36
1.2	0.726	0.274	0.38
0.9	0.327	0.673	2.06

Table 4.4: Polymerization and Chain Length for 1.2 and 0.9 C/S C-S-H

	1.2 C/S	**0.9 C/S**
Degree of polymerization	1.274	1.673
Mean chain length	2.75	6.11

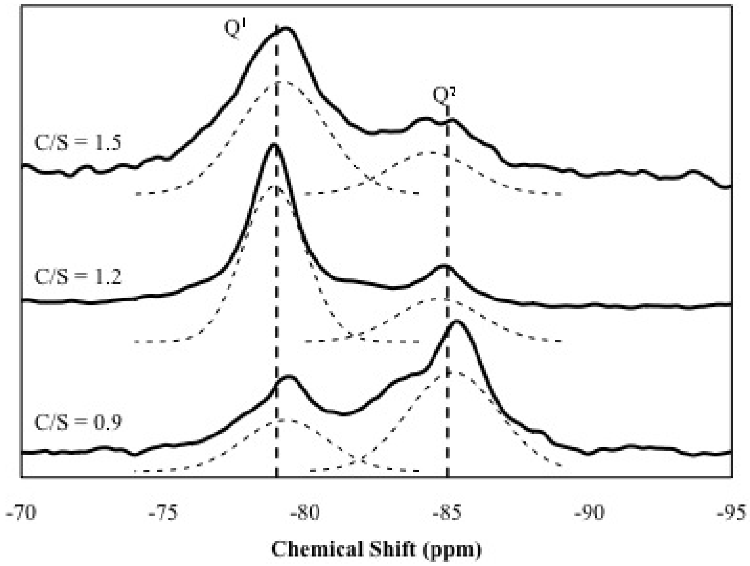

Figure 4.18: ^{29}Si NMR of C-S-H at C/S Ratios of 0.9, 1.2, and 1.5

Thermogravimetric analysis of the 1.2 C/S C-S-H shows 4.9% CH and 1.2% $CaCO_3$, meaning 93.9% of the sample is pure C-S-H (Figure 4.19). TG analysis of the 0.9 C/S C-S-H shows 6.6% CH and 1.4% $CaCO_3$, meaning 91.9% purity of the C-S-H (Figure 4.20).

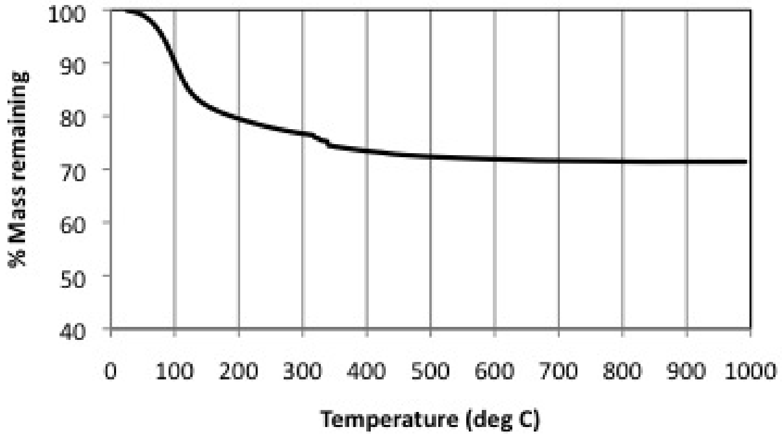

Figure 4.19: Thermogravimetric Analysis of 1.2 C/S C-S-H

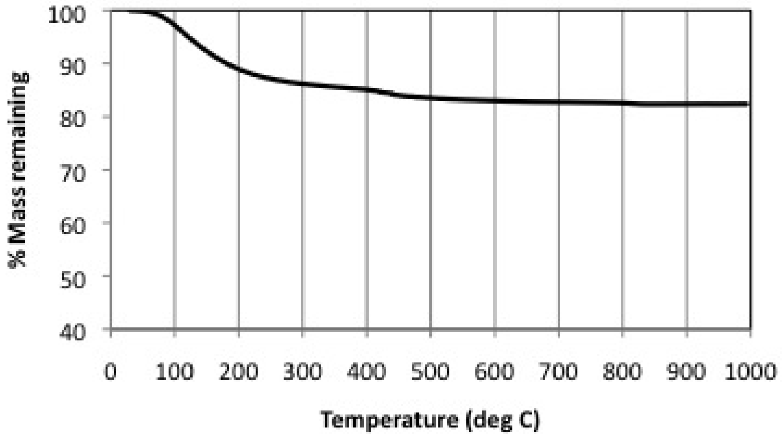

Figure 4.20: Thermogravimetric Analysis of 0.9 C/S C-S-H

The 1.2 C/S C-S-H shows an increase in elastic modulus as density increases. The difference between 95 MPa and 150 MPa is not significant, but further increase in density increased the modulus of elasticity significantly (Figure 4.21). However, the trend in the 0.9 C/S C-S-H is reversed. Increasing pressure reduced the elastic modulus significantly (Figure 4.22). While the trend in 1.2 C/S C-S-H is somewhat similar to that of 1.5 C/S, the trend in 0.9 C/S C-S-H is completely reversed. Alizadeh [6] reported a similar observation. Using dynamic mechanical analysis, it was observed that for C-S-H with a low C/S ratio (in this case 0.8), there was a discontinuous jump in elastic modulus for the higher density specimen. While a full explanation needs further in-depth investigations and more replication of tests, we offer a possible explanation related to silicate polymerization. The reduction in C/S ratio resulted in a dramatic change in silicate polymerization (see Figure 4.18 and Table 4.3). The significant increase in Q^2 bond might result in increasing high-density C-S-H. However, adding compaction pressure might damage and alter this high density material to low density C-S-H. The points in Figures 4.21 and 4.22 are the values of elastic modulus observed for distinct phases, sized relative to their relative surface fractions.

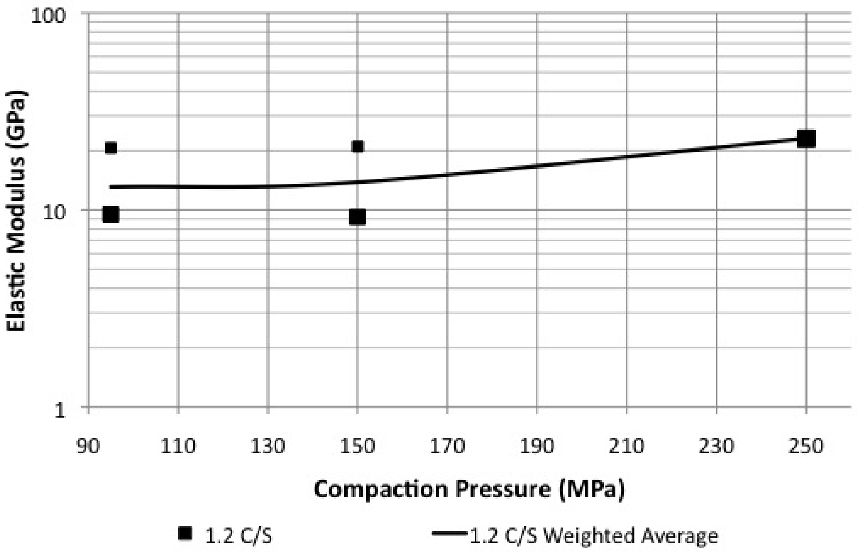

Figure 4.21: Elastic modulus versus compaction pressure for C-S-H with 1.2 C/S ratio

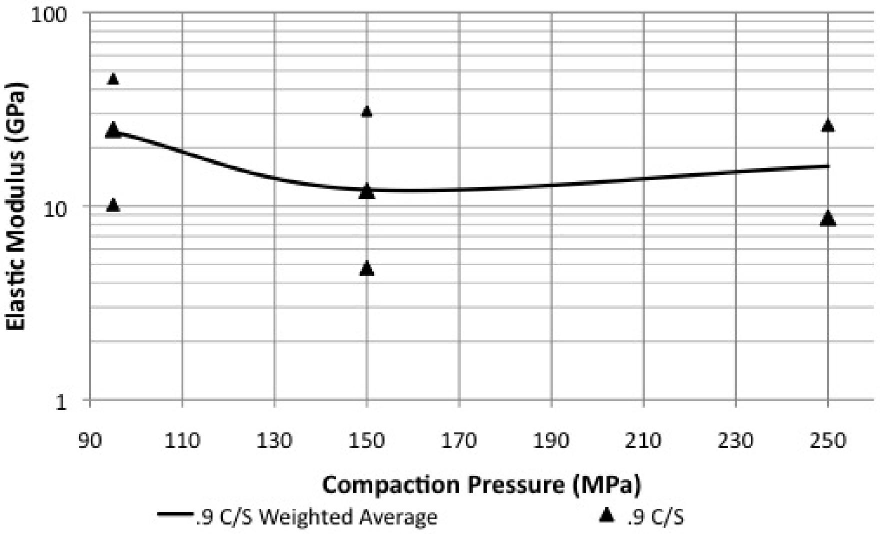

Figure 4.22: Elastic modulus versus compaction pressure for C-S-H with 0.9 C/S ratio

Table 4.5: Surface fractions and Young's modulus for 11%RH C-S-H with C/S ratios of 0.9 and 1.2

Compaction Pressure	CSH Phase Categorization	1.2 C/S		0.9 C/S	
		Surface Fraction	Youngs Modulus (GPa)	Surface Fraction	Youngs Modulus (GPa)
95 MPa	VLD	68.0%	9.5 ± 3.7	35.0%	10.2 ± 5.2
	LD	32.0%	20.6±3.5	44.0%	24.9±4.3
	HD	0.0%	N/A	21.0%	45.5±3.1
150 MPa	VLD	61.0%	9.2±2.9	38.0%	4.8 ± 3.4
	LD	39.0%	21.0± 4.0	47.0%	12.0 ± 6.5
	HD	0.0%	N/A	15.0%	31.0 ± 4.4
250 MPa	VLD	0.0%	N/A	58.0%	8.7± 4.0
	LD	100.0%	23.0 ± 8.0	42.0%	26.2 ± 5.8

Table 4.6: Weighted Elastic Average Modulus Values for 0.9 and 1.2 C/S C-S-H

Compaction pressure	Weighted Average Elastic Modulus (GPa)	
	1.2 C/S	0.9 C/S
95 MPa	13.1	24.1
150 MPa	13.8	12.1
250 MPa	23.0	16.1

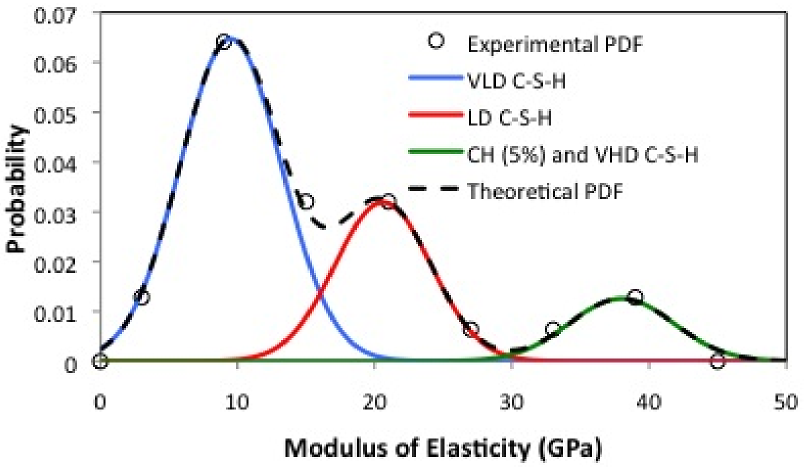

Figure 4.23: Deconvolution of 1.2 C/S C-S-H compacted to 95 MPa

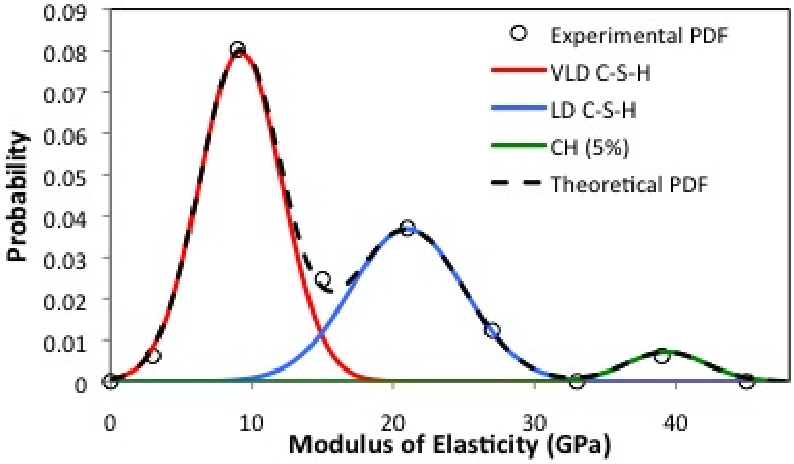

Figure 4.24: Deconvolution of 1.2 C/S C-S-H compacted to 150 MPa

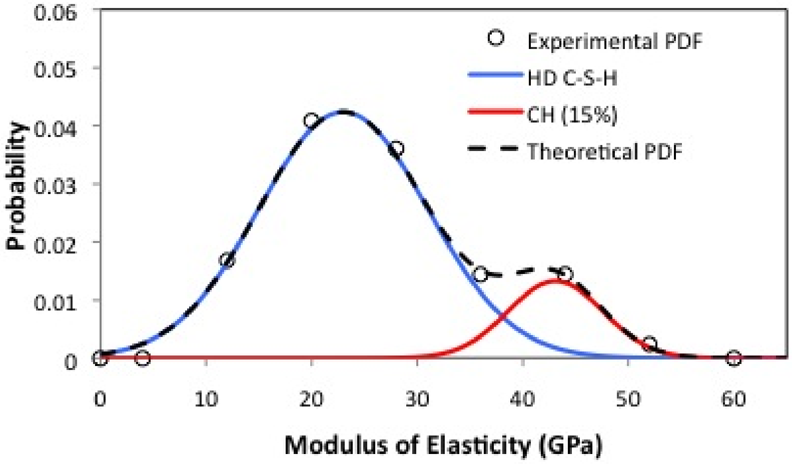

Figure 4.25: Deconvolution of 1.2 C/S C-S-H compacted to 250 MPa

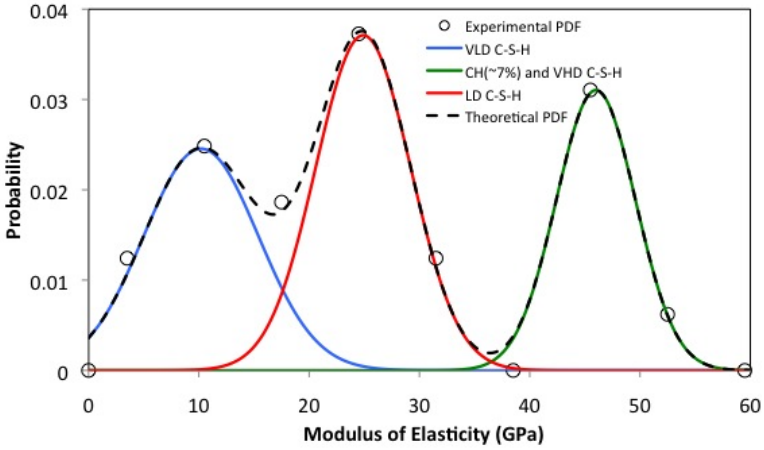

Figure 4.26: Deconvolution of 0.9 C/S C-S-H compacted to 95 MPa

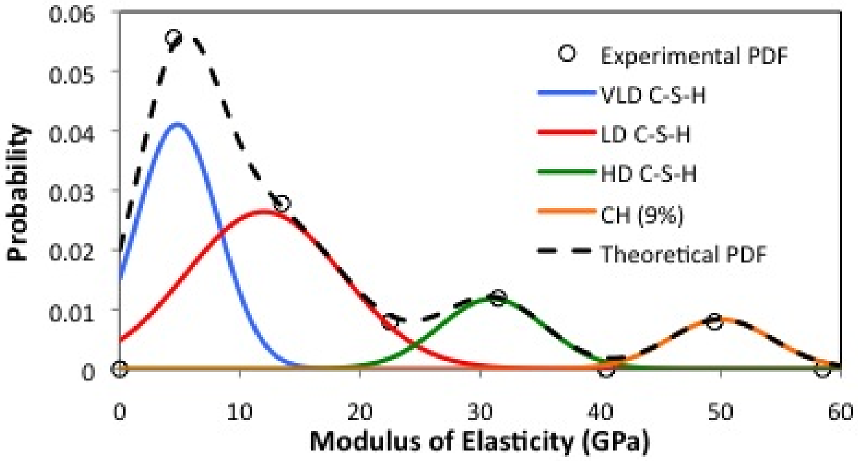

Figure 4.27: Deconvolution of 0.9 C/S C-S-H compacted to 150 MPa

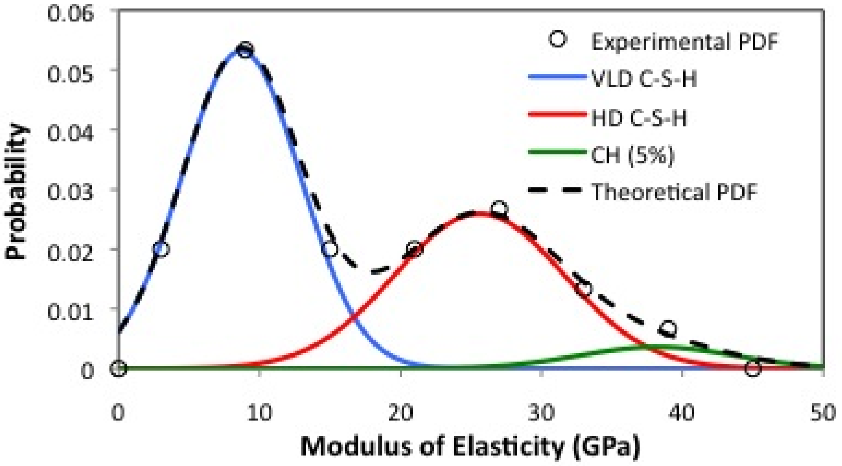

Figure 4.28: Deconvolution of 0.9 C/S C-S-H compacted to 250 MPa

4.3 1.5 C/S C-S-H Cured Under High Pressure and Temperature

Density of the 1.5 C/S C-S-H cured under elevated pressure and temperature (80°C and 10 MPa) showed that the densities were much higher than that of the normally cured 1.5 C/S C-S-H (Figure 4.29). The increase in density of the 1.5 C/S C-S-H under high temperature and pressure might be attributed to increased silicate polymerization, as observed by NMR, enabling denser C-S-H sheets and thus higher density over the C-S-H cured under ambient conditions.

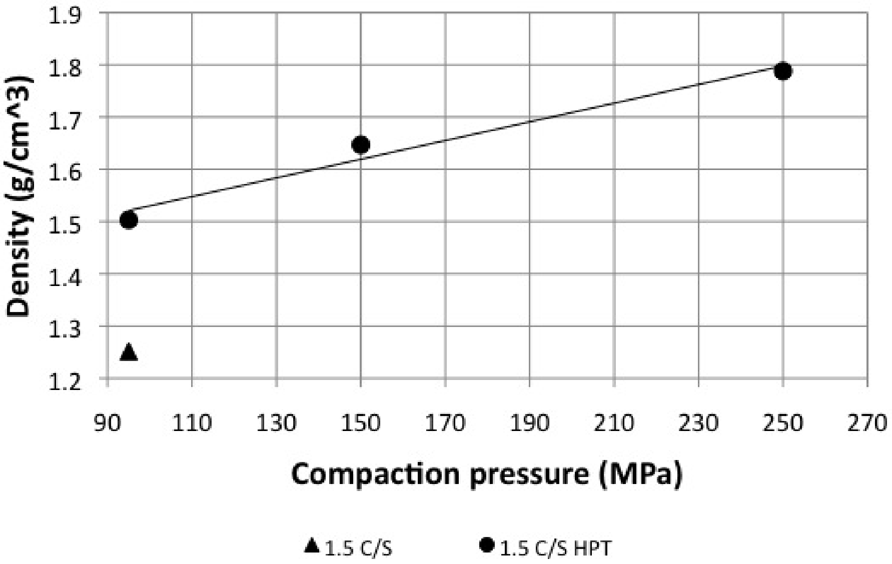

Figure 4.29: Compaction pressure versus density curve of C-S-H with a 1.5 C/S ratio cured under high temperature and pressure.

XRD analysis of C-S-H cured under high temperature and pressure showed weaker peaks than the normally cured C-S-H samples (Figures 4.3, 4.16, and 4.17), as evidenced in the plot by the relatively larger residual sample holder peak (Figure 4.30). However, the peaks for C-S-H occurred in the same locations for both normal curing and elevated curing conditions. Unlike the normally cured 1.5 C/S C-S-H, which had several large peaks of CH present (Figure 4.3), the high pressure-cured C-S-H only showed only peaks for C-S-H. The elevated temperature and pressure conditions clearly aided in the reaction of otherwise excess CaO to form a higher C/S ratio C-S-H.

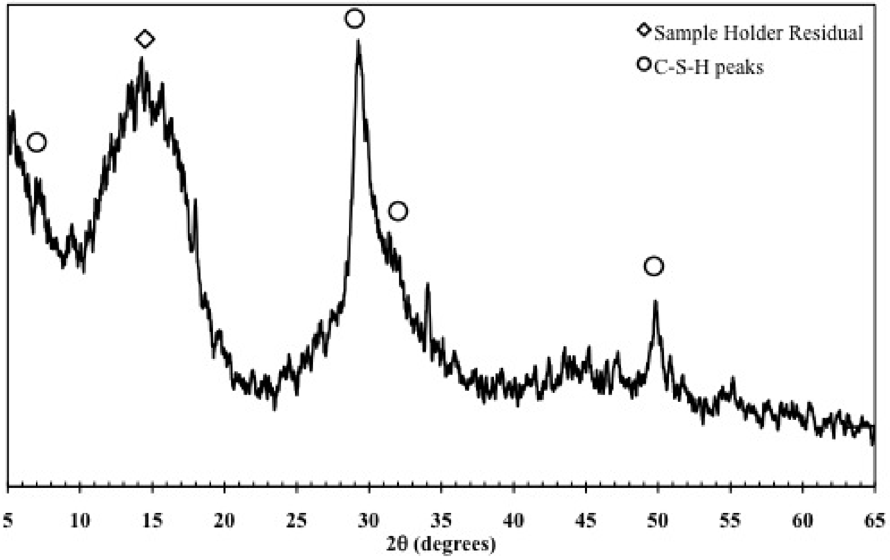

Figure 4.30: XRDA Plot of 1.5 C/S C-S-H made under high pressure and temperature.

^{29}Si NMR of the high pressure-cured C-S-H shows an increase in polymerization over the normally cured specimen with the same C/S ratio (Figure 4.31 and Table 4.8). In fact, the Q^2/Q^1 ratio was almost doubled. This increase in Q^2 polymerization has been observed to contribute to increasing stiffness, as will be shown and discussed in the following pages. However, as seen in section 4.2, the specimen made with C/S ratio of 0.9 is actually more polymerized than the high pressure 1.5 C/S sample. Degree of polymerization of the high pressure sample was 1.406, compared to the degree of polymerization of 1.673 for the 0.9 C/S specimen. The 1.5 C/S ratio is a hazy middle ground for tobermorite and jennite structures; neither curing condition produces C-S-H with a structure, indicated by mean chain length, similar to either tobermorite or jennite [28].

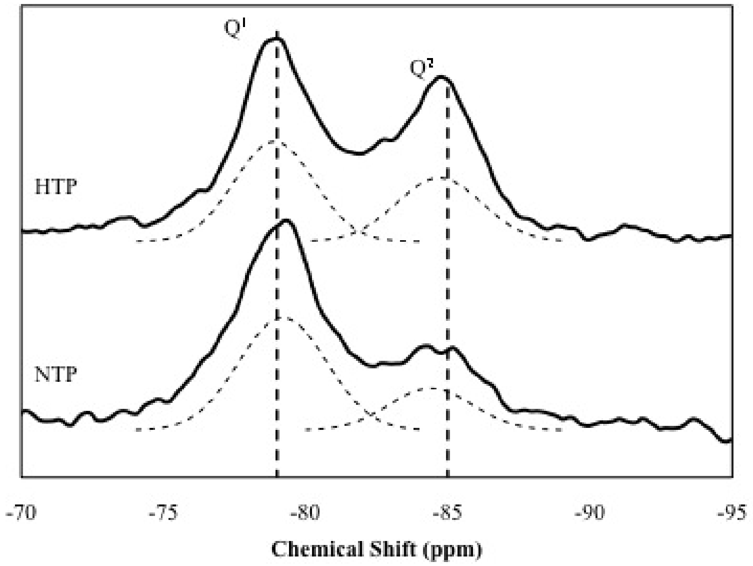

Figure 4.31: ^{29}Si NMR of C-S-H with 1.5 C/S ratio, both normally cured and cured under elevated temperature and pressure.

Table 4.7: Q^1 and Q^2 volume fractions of 1.5 C/S C-S-H for both curing conditions

Curing Condition	$\mathbf{Q^1}$	$\mathbf{Q^2}$	$\mathbf{Q^2/Q^1}$
High pressure/temperature	0.594	0.406	0.68
Normal pressure/temperature	0.738	0.262	0.36

Table 4.8: Polymerization and Chain Length for 1.5 C/S C-S-H under normal and elevated curing conditions

	Normal Curing	**Elevated Curing**
Degree of polymerization	1.261	1.406
Mean chain length	2.71	3.37

Thermogravimetric analysis of the high pressure-cured C-S-H shows 7.8% CH and just 0.7% $CaCO_3$, meaning the C-S-H is 91.5% pure (Figure 4.32), almost identical to the 1.5 C/S C-S-H made under normal curing conditions.

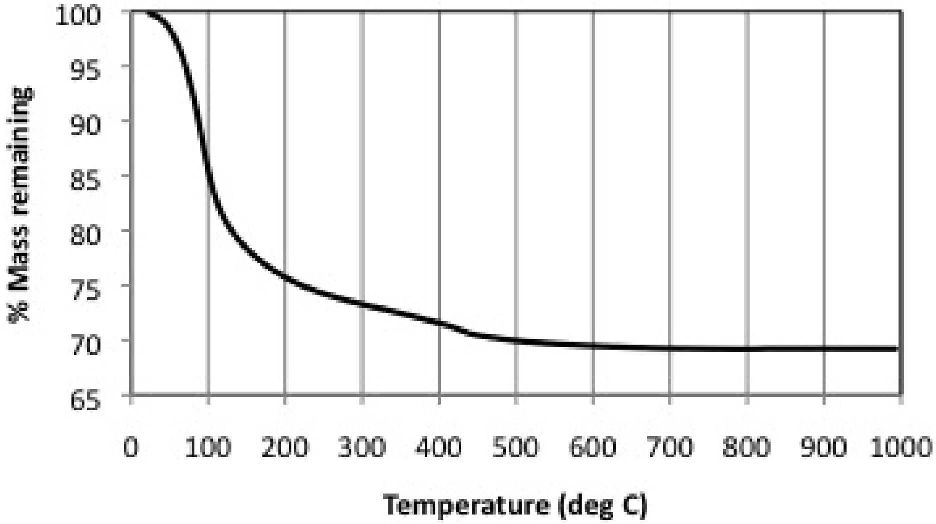

Figure 4.32: Thermogravimetric Analysis of 1.5 C/S C-S-H made under high temperature and pressure

Nanoindentation results for C-S-H cured under elevated conditions did not show a positive change in elastic response (Figure 4.33, Table 4.9), and were actually very close to the same values obtained from the normally cured 1.5 C/S C-S-H. Both specimens tested showed a high concentration of material with elastic moduli between 20 and 40 (Figures 4.34 and 4.35).

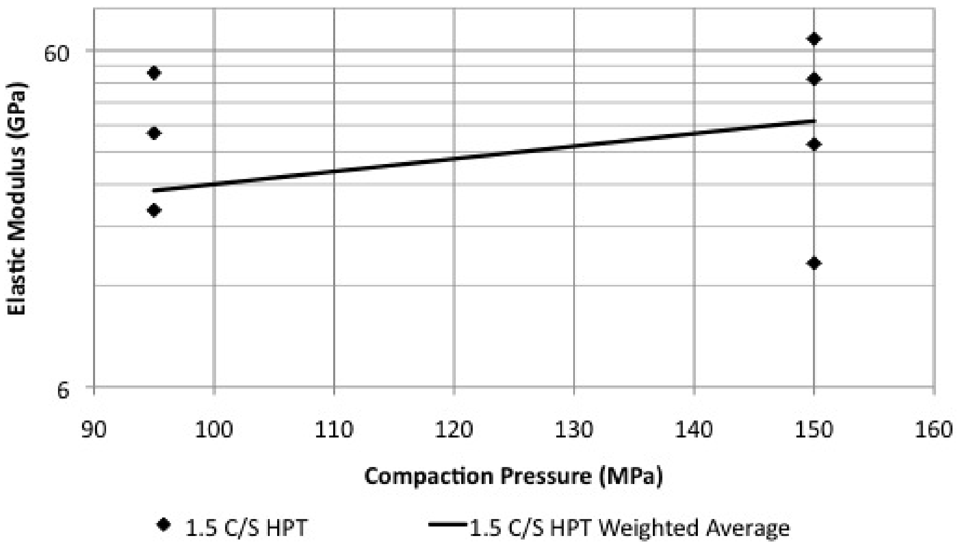

Figure 4.33: Elastic modulus versus compaction pressure for C-S-H with 1.5 C/S ratio, normal and elevated curing conditions

Table 4.9: Surface fractions and Young's modulus for 11%RH C-S-H with C/S ratio of 1.5, cured under elevated temperature and pressure

Compaction Pressure	CSH Phase Categorization	Surface Fraction	Youngs Modulus (GPa)	Weighted Avg Youngs Modulus (GPa)
95 MPa	VLD	17.0%	4.9 ± 3.6	23.0
	LD	50.0%	20.1±5.8	
	HD	28.0%	34.1±5.6	
	VHD	5.0%	51.5±4.1	
150 MPa	LD	17.0%	14.0 ± 7.5	37.0
	HD	40.0%	31.6 ± 4.6	
	VHD	38.0%	49.4 ± 5.6	
	VHD	5.0%	65.0 ± 4.6	

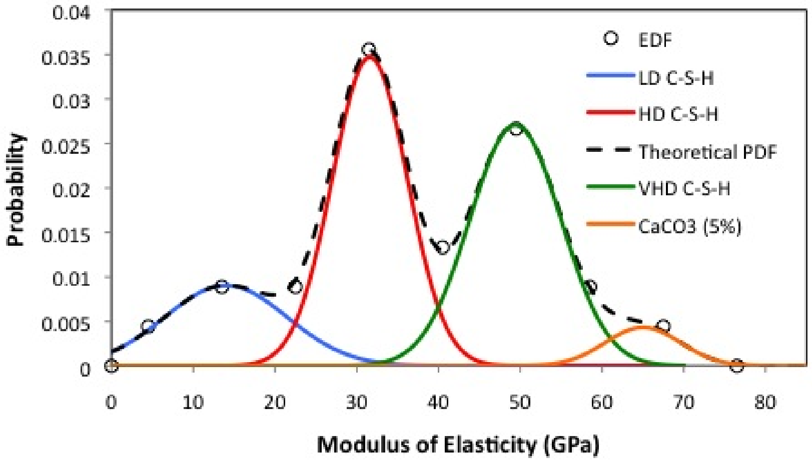

Figure 4.34: Deconvolution of 1.5 C/S C-S-H cured under high temperature and pressure, compacted to 150 MPa

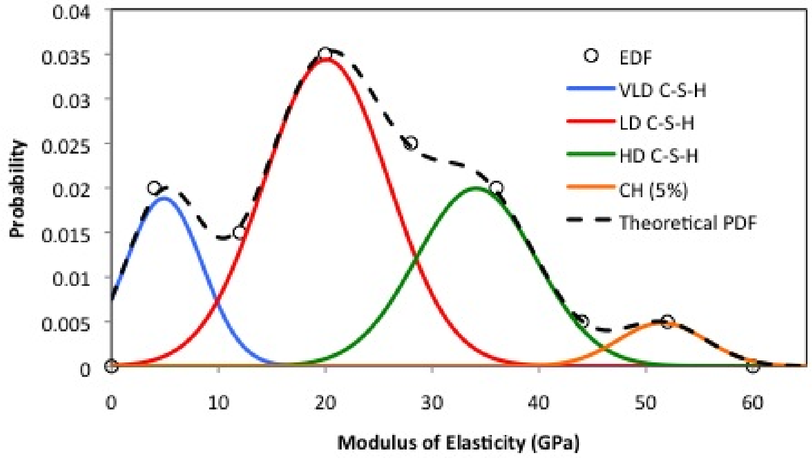

Figure 4.35: Deconvolution of 1.5 C/S C-S-H cured under high temperature and pressure, compacted to 95 MPa

A direct correlation between elastic modulus and degree of polymerization was observed for the low density 95 MPa compaction level (Figures 4.36 and 4.37). With increasing polymerization, the weighted average elastic modulus of the C-S-H is also increased. Conversely, at the high density 250 MPa compaction level, the increased polymerization has an inverse effect on the stiffness of C-S-H. The higher the polymerization, the lower the weighted average elastic modulus becomes. This is easily seen by comparing Figure 4.36 to Figure 4.38, and also is supported by findings in the literature [6]. The vertical black bars shown in Figures 4.37 and 4.38 show the maximum and minimum observed values.

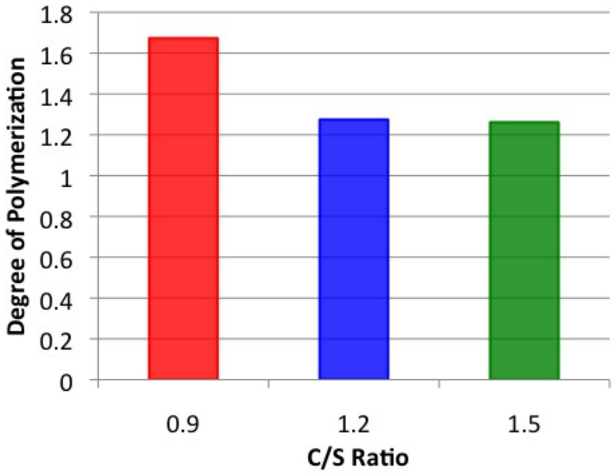

Figure 4.36: Degree of polymerization for normally cured C-S-H

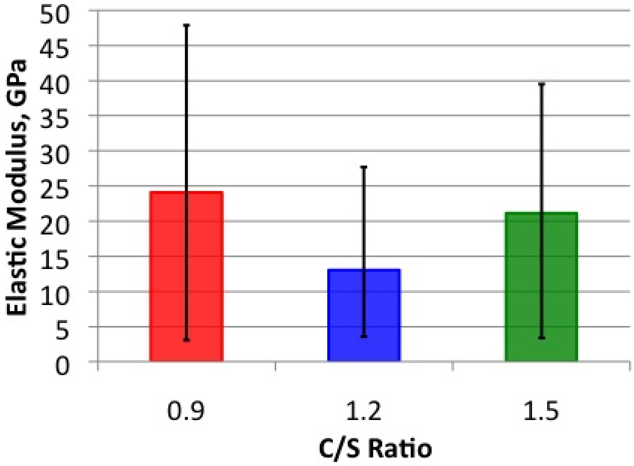

Figure 4.37: Weighted average elastic modulus of C-S-H compacted to 95 MPa

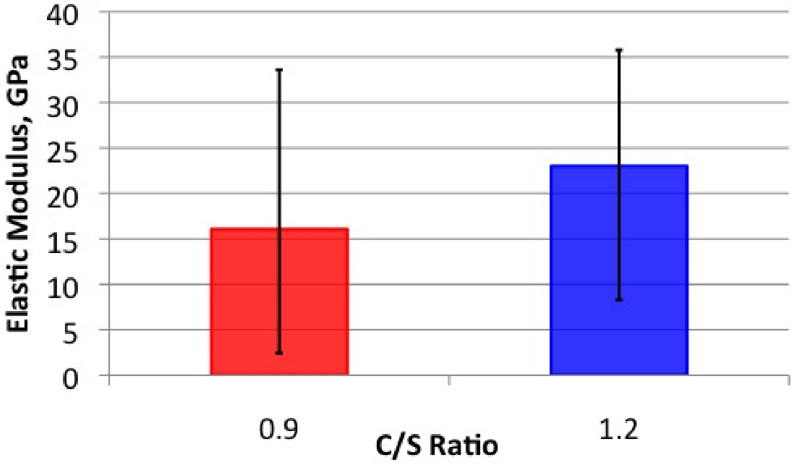

Figure 4.38: Weighted average elastic modulus of C-S-H compacted to 250 MPa

Elevated curing conditions also caused an increase in polymerization (Figure 4.39), as expected. The increase in temperature and pressure activates the silicate connections, causing them to become more reactive and bond with additional CaO. This increased polymerization in turn caused the C-S-H to become stiffer at low density (Figure 4.40) as occurred for the normally cured C-S-H. Again, the black vertical bars shown in Figure 4.40 indicate the maximum and minimum observed values from the tests.

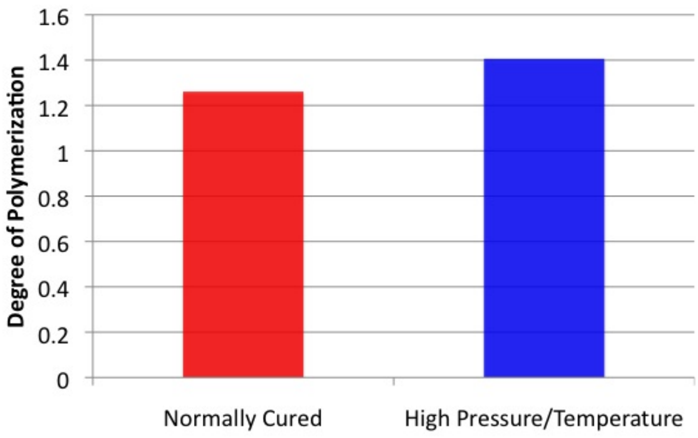

Figure 4.39: Degree of polymerization for 1.5 C/S C-S-H under both curing conditions

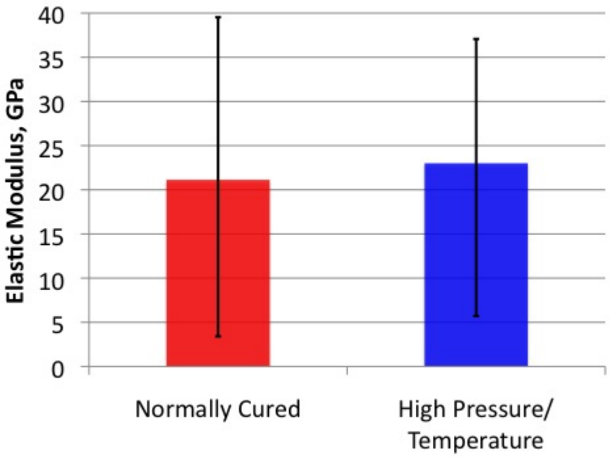

Figure 4.40: Weighted average elastic modulus of C-S-H compacted to 95 MPa, 1.5 C/S

Chapter 5

Conclusions and Recommendations

The experiments presented systematic methods for synthesis, drying, and characterization of C-S-H. The experiments were performed on C-S-H synthesized at three C/S ratios: 1.5, 1.2, and 0.9, as well as a batch synthesized with a C/S ratio of 1.5 and cured at a pressure of 10 MPa and temperature of 80°C. The XRD and ^{29}Si NMR analyses proved the formation of C-S-H with typical peaks reported in the literature. The NMR analysis showed that under normal curing conditions, only Q^1 and Q^2 silicon bonds are observed, indicating no unreacted silica (which would have produced Q^0 peaks). The high pressure-cured C-S-H showed a large increase in Q^2 bond, as did the 0.9 C/S C-S-H. XRD analysis showed that decreasing the C/S ratio decreased the amount of CH present, as expected. Curing under elevated temperature and pressure also proved to decrease CH content, as increased reactivity of the silica was activated by the elevated curing conditions.

The compaction process was more successful with the 11%RH C-S-H which seems to have enough water to lubricate the C-S-H layers and produce higher density with compaction than the d-dry C-S-H. The low density and high dryness of the d-dry material was reflected in the modulus of elasticity observations, which were all lower than the 11%RH conditioned material. From the initial testing on 1.5 C/S C-S-H, it became obvious that compaction pressures greater than 95 MPa were needed to create a C-S-H with density and properties comparable to that of C-S-H in-situ in hydrated cement. The subsequent batches were compacted to 95, 150, and 250 MPa and showed densities inline with expected values from literature.

Nanoindentation of synthetic C-S-H is reported, and methodology to analyze nanoindentation observations based on statistical deconvolution is described and used. We present the first results on mechanical properties extracted at the nanoscale from synthetic C-S-H rather than hydrated cement, as has previously been done in the literature. There is a clear correlation between degree of polymerization and elastic modulus at lower densities. Increased polymerization under normal curing conditions has been observed to make the C-S-H stiffer at low density. Conversely at higher densities, increased polymerization makes the C-S-H less stiff.

When the curing conditions are elevated (80°C and 10 MPa were used in this study), the polymerization of the C-S-H is noticeably increased over normally cured C-S-H for an identical C/S ratio. This increase makes the C-S-H stiffer when at a low density, as was also observed for the normally cured C-S-H with varying C/S ratios. Further research is needed to further explain and define this relationship.

The primary contribution of this research to the scientific community is the basis of understanding of elastic properties of C-S-H as a function of C/S ratio and degree of polymerizartion. While other researchers [12, 7, 5, 6] have synthesized C-S-H using various methods, no research to date has presented nano-scale mechanical properties of phase-pure C-S-H. This investigation of mechanical properties combined with the chemical analysis provide an important basis for future work and development of “concrete by design”.

Considerable work in this thesis was founded on the desire of coming to a systematic, consistent, and repeatable method for producing C-S-H. Upcoming work shall include further mechanical characterization of C-S-H including fracture toughness testing. This will help to determine which if any C/S ratio provides the most resistance to microcrack growth. Work should also be done on additional compaction levels to further define the relationship between density, polymerization, and elastic modulus. Future research on elastic properties should also focus on spherical indentation instead of Berkovich indentation. Spherical indentation can also provide data on creep of C-S-H as a function of density and C/S ratio, which is important information to understand time dependent behavior of C-S-H. Other future work might include efforts to alter C-S-H by incorporating other materials such as nanoclay, polymers, and carbon nanotubes. Efforts to replace lime by other geomaterials might also be interesting.

References

[1] HFW Taylor. *Cement Chemistry*, volume 1. Thomas Telford Publishing, London, 2 edition, 1997.

[2] JF Young and W Hansen. Volume relationships for C-S-H formation based on hydration stoichiometries. In L. Strubel and P. Brown, editors, *Materials Research Symposium*, volume 85, pages 313–322, Pittsburgh, PA, 1987. Materials Research Society.

[3] AM Neville and JJ Brooks. *Concrete Technology*, volume 1. Longman Singapore Publishers Ltd, Singapore, 1987.

[4] PK Mehta and PJM Monteiro. *Concrete Microstructure, Properties, and Materials*. McGraw-Hill, 3 edition, 2006.

[5] D Sugiyama. Chemical alteration of calcium silicate hydrate (C-S-H) in sodium chloride solution. *Cement and Concrete Research*, 38:1270–1275, 2008.

[6] R Alizadeh and JJ Beaudoin. Mechanical properties of calcium silicate hydrates. *Materials and Structures*, 44:13–28, 2011.

[7] X Cong and RJ Kirkpatrick. 29Si MAS NMR study of the structure of calcium silicate hydrate. *Advanced Cement Based Materials*, 3:144–156, 1996.

[8] M Atkins, FP Glasser, and A Kindness. Cement hydrate phases: Solubility at 25C. *Cement and Concrete Research*, 22(1):6, 1992.

[9] G Constantinides and FJ Ulm. The effect of two types of C-S-H on the elasticity of cement-based materials: Results from nanoindentation and micromechanical testing. *Cement and Concrete Research*, 34:67–80, 2004.

[10] PD Tennis and HM Jennings. A model for two types of calcium silicate hydrate in the microstructure of portalnd cement pastes. *Cement and Concrete Research*, 30:855–863, 2000.

[11] HM Jennings. Colloid model of C-S-H and implications to the problem of creep and shrinkage. *Materials and Structures*, 37:59–70, 2004.

[12] JJ Beaudoin and RF Feldman. Dependence of degree of silica polymerization and intrinsic mechanical properties of C-S-H on c/s ratio, 9/22/1986 1986.

[13] HFW Taylor. The calcium Silicate Hydrates. In HFW Taylor, editor, *The Chemistry of Cements*, pages 168–232. Academic Press Inc., New York, 1964.

[14] RF Feldman and VS Ramachandran. Differentiation of interlayer and adsorbed water in hydrated portland cement by thermal analysis. *Cement and Concrete Research*, 1:607–620, 1971.

[15] LE Copeland and JC Hayes. Determination of non-evaporable water in hardened portland-cement paste. *ASTM Bulletin*, pages 70–74, 1953.

[16] DL Kantro, S Brunauer, and CH Weise. Development of surface in the hydration of calcium silicates. *Advances in Chemistry Series*, 33:199–219, 1962.

[17] I Odler and H Dorr. Early hydration of tricalcium silicate i. kinetics of the hydration process and the stoichiometry of the hydration products. *Cement and Concrete Research*, 9:239–248, 1979.

[18] C Alonso and L Fernandez. Dehydration and rehydration processes of cement paste exposed to high temperature environments. *Journal of Materials Science*, 39:3015–3024, 2004.

[19] L Alarcon-Ruiz, G Platret, E Massieu, and A Ehrlacher. The use of thermal analysis in assessing the effect of temperature on a cement paste. *Cement and Concrete Research*, 35:609–613, 2005.

[20] JB Odelson, EA Kerr, and W Vichit-Vadakan. Young's modulus of cement paste at elevated temperatures. *Cement and Concrete Research*, 37:258–263, 2007.

[21] J Jain and N Neithalath. Physico-chemical changes in nano-silica and silica fume modified cement pastes in response to leaching. *International Journal of Materials and Structural Integrity*, 3(2/3):114–133, 2009.

[22] CM Earnest. *Compositional Analysis by Thermogravimetry.* ASTM Special Technical Publications, Philadelphia, 1988.

[23] M Magi, E Lippmaa, and A Samoson. Solid-state high-resolution silicon-29 chemical shifts in silicates. *Journal of Physical Chemistry*, 88:1518–1522, 1984.

[24] JF Young. Investigations of calcium silicate hydrate structure using silicon-29 nuclear magnetic resonance spectroscopy. *Journal of the American Ceramic Society*, 71(3):C118–C120, 1988.

[25] JJ Beaudoin, L Raki, and R Alizadeh. A 29Si MAS NMR study of modified C-S-H nanostructures. *Cement and Concrete Composites*, 31:585–590, 2009.

[26] G Le Saout, E Lecolier, A Rivereau, and H Zanni. Chemical structure of cement aged at normal and elevated temperatures and pressures, part I: Class G oilwell cement. *Cement and Concrete Research*, 36:71–78, 2006.

[27] G Le Saout, E Lecolier, A Rivereau, and H Zanni. Chemical structure of cement aged at normal and elevated temperatures and pressures, part II: Low permeability class G oilwell cement. *Cement and Concrete Research*, 36:428–433, 2006.

[28] HFW Taylor. Proposed structure for calcium silicate hydrate gel. *Journal of the American Ceramic Society*, 69(6):464–467, 1986.

[29] P Mondal, SP Shah, and LD Marks. Nanoscale characterization of cementitious materials. *ACI Materials Journal*, (March-April):174–179, 2008.

[30] M Miller, C Bobko, M Vandamme, and FJ Ulm. Surface roughness criteria for cement paste nanoindentation. *Cement and Concrete Research*, 38:467–476, 2008.

[31] G Constantinides and FJ Ulm. The nanogranular nature of C-S-H. *Journal of the Mechanics and Physics of Solids*, 55:64–90, 2007.

[32] AC Fischer-Cripps. *Nanoindentation*. Springer Science+Business Media, LLC, New York, 2 edition, 2004.

[33] G Constantinides, FJ Ulm, and K Van Vliet. On the use of nanoindentation for cementious materials. *Materials and Structures*, 36(April):191–196, 2003.

[34] P Acker. Micromechanical analysis of creep and shrinkage mechanisms. In FJ Ulm, ZP Bazant, and FH Wittmann, editors, *Creep, shrinkage, and durability mechanics of concrete and other quasi-brittle materials*, pages 15–25, Cambridge, MA, 2001. Elsevier Science.

[35] S Igarashi, A Bentur, and S Mindess. Characterization of the microstructure and strength of cement paste by microhardness testing. *Advances in Cement Research*, 8(30):87–92, 1996.

[36] HM Jennings. A model for the microstructure of calicum silicate hydrate in cement paste. *Cement and Concrete Research*, 30:101–116, 2000.

[37] JJ Thomas, HM Jennings, and AJ Allen. The surface area of cement paste as measured by neutron-scattering-evidence for two C-S-H morphologies. *Cement and Concrete Research*, 28(6):897–905, 1998.

[38] ASTM Standard E 104-02: Standard practice for maintaining constant relative humidity by means of aqueous solution. ASTM International, West Conshohocken, PA, 2007.

[39] J Zhang, EA Weissinger, S Peethamparan, and GW Scherer. Early hydration and setting of oil well cement. *Cement and Concrete Research*, 40:1023–1033, 2010.

[40] ASTM Standard C 914-95: Standard test method for bulk density and volume of solid refractories by wax immersion. ASTM International, 2004.

[41] JJ Beaudoin. Comparison of mechanical properties of compacted calcium hydroxide and portland cement paste systems. *Cement and Concrete Research*, 13(3):319–324, 1983.

[42] R Alizadeh. *Nanostructure and engineering properties of basic and modified calcium-silicate-hydrate systems.* Phd, University of Ottawa, 2009.

[43] A Nonat and X Lecoq. The structure, stoichhiometry, and properties of C-S-H prepared by C3S hydration under controlled condition. *Nucelar magnetic resonance spectroscopy of cement-based materials*, pages 197–207, 1998.